Combustion and Flame 258 (2023) 113039

Contents lists available at ScienceDirect

Combustion and Flame

journal homepage: www.elsevier.com/locate/combustflame

A DNS evaluation of three MMC-like mixing models for transported PDF modelling of turbulent nonpremixed flames

Zisen Li[a,c,*], Evatt R. Hawkes[a], Armin Wehrfritz[b], Bruno Savard[c]

[a] School of Mechanical and Manufacturing Engineering, University of New South Wales, Sydney, NSW 2052, Australia
[b] Mechanical Engineering, University of Turku, Turku 20014, Finland
[c] Department of Mechanical Engineering, Polytechnique Montréal, Montréal H3T 1J4, Canada

ARTICLE INFO

Article history:
Received 10 April 2023
Revised 18 August 2023
Accepted 20 August 2023

Keywords:
Transported probability density function
Molecular mixing model
Multiple mapping conditioning
DNS Evaluation
Turbulent nonpremixed flames

ABSTRACT

Transported probability density function (TPDF) methods are suitable for modelling turbulent reactive flows. One of the main challenges is to accurately model the molecular mixing terms. In TPDF mixing models, it is desired that the principle of localness is satisfied so that the molecular mixing is performed locally in both physical and composition spaces. The multiple mapping conditioning (MMC) mixing model can ensure mixing localness without violating other desired principles. The present study examines three MMC-like mixing models, including the original MMC (OMMC) mixing model, shadow-position mixing model (SPMM) and a conceptually simplified multiple mapping conditioning (SMMC) mixing model. Three direct numerical simulation (DNS) datasets modelling turbulent nonpremixed ethylene flames with increasing levels of extinction are used for model evaluation. The DNS datasets are also used to provide both initial conditions and inputs needed over the course of TPDF runs to remove the uncertainties caused by turbulence closure, allowing the study to focus on the molecular mixing model. The mixing model coefficients are specified analytically by reference to a canonical mean scalar gradient (MSG) flow in order to achieve specifiable dissipation rate and user-controllable localness. The results show that the MMC-like mixing models yield similar prediction of flame extinction and reignition if the coefficients are properly specified. The MMC-like mixing models can also be tuned to achieve a desired level of localness. For conditional statistics, the MMC-like mixing models can yield correct level of conditional variances. By changing localness, the MMC-like models can yield solutions resembling the interaction by exchange with the mean (IEM) or Euclidean minimum spanning tree (EMST) mixing model for extreme parameter choices. The models differ in their abilities to specify unconditional dissipation rates, at least in the flow considered, and in their ease of implementation.

1. Introduction

Understanding turbulent nonpremixed combustion is important for improving the performance of aeronautical and aeroderivative gas-turbine engines, diesel engines and industrial burners [1]. The mixing rates encountered in these practical devices are often high enough so that simple fast-chemistry approximations are inadequate and methods that can handle situations where mixing and reaction timescales overlap are required. Nonpremixed flames with extinction and reignition [2–4] provide a well-studied example of such a situation.

The composition transported probability density function (TPDF) method [5,6] is a modelling approach that is not limited to the fast chemistry approximation, and has proven to be a reasonably accurate and computationally tractable in the modelling of turbulent nonpremixed and other flames [7–11,11–15]. As the chemical reaction terms appear in closed form in the TPDF method, it has natural advantages in dealing with finite-rate chemical processes such as those involved in extinction and reignition. The trade off for this closure is that molecular micro-mixing is unclosed and requires modelling. A number of molecular mixing models have been proposed (see Ref. [7] for a review). Among those very relevant to this work are interaction by exchange with the mean (IEM) [16] (also known as the linear mean square estimation (LMSE) model [17]), the modified Curls (MC) model [18], the Euclidean minimum spanning tree (EMST) model [19] and

* Corresponding author.
E-mail address: zisen.li@polymtl.ca (Z. Li).

https://doi.org/10.1016/j.combustflame.2023.113039

models that fall under the multiple mapping conditioning (MMC) framework [20].

Desirable properties for a TPDF mixing model have been proposed for Reynolds-averaged Navier–Stokes (RANS) simulations [21], and for large-eddy simulations (LES) [22], including: the preservation of the mean; decay of variance; localness; linearity and independence of mixing; amongst others. It should be noted that none of the existing models possesses all of the desirable properties (which also include desirables such as dependence on other parameters such as Reynolds number, etc), however, some are constructed to satisfy the most important ones, particularly those listed above. In the present work, the main focus is put on the property of localness. Localness means that the mixing of Pope particles [23] should be local in composition space, as a proxy for the physical process of molecular mixing which in the continuum limit is a spatially local process depending on composition gradients.

The localness property is important for combustion modelling. For instance, considering combustion in the flamelet regime, a non-local model could allow mixing between particles on the fuel-rich side of the reaction zone with particles on the fuel-lean side, resulting in cold, non-reacting particles within the reaction zone and thus spurious extinction, e.g., see Norris and Pope [24]. Academic test cases such as those used in Ref. [24] are sufficient to expose this potential problem, but are insufficient to understand how important it is in a practical case. Failures of non-local models are also well known in comparisons to experiments [25], but it is difficult to definitely attribute the failure to the mixing model, given multiple models are being tested at the same time (including chemistry, turbulence, mixing frequency, etc.). In more recent work [26], attempts were made to use DNS to provide all inputs to a composition probability density function (PDF) model that would normally be provided by sub-models other than the mixing model. This enabled a reasonably conclusive demonstration that the prediction of extinction and reignition in the DNS (of temporally evolving, non-premixed plane-jet flames), depended strongly on the localness of the model. EMST, which is fully local, generally predicted the overall ignition behaviour but always underpredicted the variances conditional on mixture fraction (conditional variances), and particularly, never captured the bi-modal conditional PDF of reacting scalars that was seen in the DNS, while IEM and MC models, which do not ensure localness, predicted too much extinction but yielded qualitatively good agreement on the conditional variance in the sense that they at least predicted a bimodal conditional PDF. These results suggest that controllable localness might be a useful attribute of a mixing model. In stating this we emphasise that from the physical perspective, mixing is always local, however the single-point TPDF method can never fully reconstruct that except in the DNS limit, so we rely on constructing a system of stochastic differential equations that in a weak sense approximates the evolution of the PDF, without resorting to a higher level of closure. In this sense a model that is not strictly local but approximately so can potentially out perform a model that attempts to be fully local.

The MMC model [20] is a promising solution that can achieve both controllable localness and consistency with other principles such as the linearity and independence of mixing, which EMST, a very local model, violates. In the MMC model, reference variables are introduced and associated to certain flame characteristics, e.g., mixture fraction for nonpremixed flames [10,27,28] or partially premixed flames [29,30], and progress variable for premixed flames [31]. Unlike the IEM model, in which composition scalars are mixed towards the unconditional means, the MMC model performs mixing of physical scalars locally in the reference variable space; many implementations are statistically equivalent to mixing scalars with their conditional mean in reference space [8]. The mixing of scalars is therefore confined within the conditional mean manifold(s) parameterised by the reference variable, and thus local in the reference space. Generally, the mixing rate of physical scalars towards their conditional mean in reference variable space is set to be faster than the unconditional mixing rates, and this gives rise to correlations between the physical scalars and the reference variable, the strength of which controls how local the mixing model is in the physical scalar space. Completely non-local behaviour (e.g., similar to IEM or MC depending on numerical implementation), or completely local, CMC-like behaviours can be recovered for different choices, e.g., see Refs. [32,33].

Multiple variations of the MMC model have been proposed and applied in the simulation of nonpremixed [10,28,34–36], premixed [31,37,38] and partially premixed [39] flames, as well as multiphase flames [14]. Among these works, a stochastic RANS version of the MMC model [10,28,34,35] has been frequently employed in modelling of nonpremixed turbulent flames. This MMC model inherits most of the features possessed by the original stochastic version of the MMC concept as originally proposed by Klimenko and Pope [20] and is thus referred to here as the original MMC (OMMC) model. In the OMMC model, the transport equation of the reference variable is constructed in such a way that it has Gaussian statistics with zero mean and unit variance. The localness of the OMMC model can be changed by $\tau_{\min}/\tau_\phi$, which denotes the ratio of the conditional mixing time scale, $\tau_{\min}$, to the (unconditional) mixing time scale of the reference scalar, τ_ϕ. Decreasing $\tau_{\min}/\tau_\phi$, which suppresses the conditional scalar fluctuations, leads to a higher level of localness. Work to date does not appear to have revealed universal values of $\tau_{\min}/\tau_\phi$. For example, Wandel and Klimenko [32] evaluated the performance of MMC mixing model against a DNS, of which the composition field was initialised by blobs of pure fuel and air and the velocity field by homogeneous turbulence. It was suggested that the MMC mixing model with $\tau_{\min}/\tau_\phi = 0.125$ managed to predict the overall nonpremixed ignition process. The same ratio $\tau_{\min}/\tau_\phi = 0.125$ also yielded the best result for the Sydney piloted premixed jet burner (PPJB) flame [35]. Wandel [33] suggested that the value of $\tau_{\min}/\tau_\phi$ should change within the flame depending on the combustion conditions, and proposed a model to predict the value. For the Sandia nonpremixed flame series D-F, $\tau_{\min}/\tau_\phi$ has been suggested to be in the range of $0.35 - 1.0$ depending on the extinction level [10,28,34]. In this work so far, either conditions were very idealised DNS (the non-heat releasing, homogeneous, single-step chemistry DNS studied in Ref. [32]) or were comparisons to experiment, where all sub-models are tested together.

Recently, new MMC-like mixing models have been proposed, notably the shadow-position mixing model (SPMM) proposed by Pope [8], and the conceptually simplified multiple mapping conditioning model (SMMC) proposed by Varna et al. [40,41]. Together with OMMC, the SPMM and SMMC models constitute the main focus of this study. Before proceeding to discuss the SPMM and SMMC models further, we note that in this article we restrict our focus for SPMM to composition-SPMM. Pope's original article [8] mainly focusses on the more advanced velocity-composition SPMM, with composition PDF presented as an aside. We focus on composition SPMM here in order to consistently compare three composition-TPDF models, and future work may consider velocity-composition-TPDF methods.

The SPMM and SMMC models under investigation are referred to here as "MMC-like" in that they inherit the main feature of MMC, the conditioning of mixing locally in the space of a reference variable which evolves according to a stochastic differential equation. Neither of these models appears to be exactly the modelled form of MMC originally proposed by Klimenko and Pope [20], however also many subsequent interpretations of MMC are not either [42–44].

In SPMM, mixing is conditioned on a "shadow displacement", which represents an offset in physical space from the particle's real position. Pope [8] proposed SPMM originally for both velocity-composition and composition PDF frameworks, and demonstrated using canonical test cases that the models satisfy many of the desirable properties of a mixing model while offering controllable localness. In an a priori DNS study in a temporally evolving jet-flame configuration [45], the shadow displacement R was shown to be highly correlated with mixture fraction and velocity, thus showing, in a reasonably complex setting, the model's ability to enforce localness in composition space. A posteriori tests in complex cases are however currently lacking, save for preliminary work reported in Tang et al. [46].

The SMMC model, proposed by Varna et al. [40,41], introduces a reference variable, ξ, which is designed to be statistically similar to mixture fraction. Specifically, it is designed so that the mean and variance of ξ are approximately the same as that of mixture fraction in some canonical flows. It has been found that the SMMC model with high localness yielded good predictions for Sandia Flame D-F [41] and the ECN Spray A case, a reference flame for diesel [47].

Summarising the above, the considered MMC-like models (OMMC, SPMM and SPMM) have potential based on their favourable properties, and some demonstrated successes, however no study to our knowledge ever compared and evaluated these models together in any setting. This comparison and evaluation is the main objective of this paper. In addition, the comparison will be done against DNS data, and, following a number of previous studies in our group [26,46–48], all inputs to the TPDF solver normally needed from a turbulence model (i.e. the mixing frequency, the turbulent diffusion coefficient, and the mean flow velocity) will be provided directly by the DNS. This type of comparison eliminates considerable uncertainties, enabling a more precise focus on the evaluation of mixing models.

One difficulty in carrying out such a comparison is that the models all have some user-specifiable constants which are not directly comparable between models. We circumvent this problem by proposing a unified approach to setting the constants for a simple idealised flow involving a uniform scalar gradient interacting with homogeneous isotropic turbulence, in which the models have an analytic solution. In particular, we set the constants for each model so that the implied unconditional dissipation rate of mixture fraction variance and the correlation coefficient between mixture fraction and the reference variable both tend towards user-specified values in the considered flow.

The rest of the present work is organised as follows. The TPDF methodology is introduced in Section 2. The results are presented and discussed in Section 3. Conclusions are drawn in Section 4.

2. TPDF methodology

The composition TPDF method solves the evolution of Eulerian Favre-joint PDF, $\widetilde{f}_\phi$, of the composition scalars ϕ_k, which typically includes mass fractions of $N_{\rm sp}$ chemical species and an energy variable (e.g., enthalpy). In other works, see [7], these variables can be combined with velocity to create a velocity-composition PDF framework, or with other variables such as pressure, turbulence frequency, and so on, resulting in more sophisticated models. However, in the present work, focus is restricted to composition PDF methods and "TPDF" and "PDF" refer to this.

In this section, conventional TPDF methods are introduced and their solution by a Lagrangian particle approach is outlined in overview. Following that, the three MMC-like methods that are considered here are introduced.

2.1. Conventional PDF methods and Lagrangian particle method

In a framework of Favre averaging in the RANS context, the governing equation for $\widetilde{f}_\phi$ is:

$$\frac{\partial}{\partial t}\left[\langle\rho\rangle\widetilde{f}_\phi\right]+\frac{\partial}{\partial x_j}\left[\langle\rho\rangle\widetilde{u}_j\widetilde{f}_\phi\right]+\langle\rho\rangle\frac{\partial}{\partial\psi_k}\left[S_k\widetilde{f}_\phi\right]$$
$$=-\frac{\partial}{\partial x_j}\left[\langle\rho\rangle\langle u_j''|\psi_k\rangle\widetilde{f}_\phi\right]+\frac{\partial}{\partial\psi_k}\left[\left\langle\frac{1}{\rho}\frac{\partial J_j^k}{\partial x_j}|\psi_k\right\rangle\langle\rho\rangle\widetilde{f}_\phi\right] \quad (1)$$

Here, the Favre-average of ϕ_k is denoted as $\widetilde{\phi}_k=\langle\rho\phi_k\rangle/\langle\rho\rangle$, where ρ is the fluid density and $\langle\cdot\rangle$ is the Reynolds-average operator. The quantities, $\widetilde{u}_j$ and u_j'' are the Favre mean and fluctuation velocity components, respectively; S_k, J_j^k and ψ_k represent the chemical reaction, diffusion flux tensor and the sample space variables of ϕ_k, respectively.

2.1.1. Particle method

Equation (1) is typically high-dimensional ($N_{\rm sp}\sim 10^1-10^3$) and thus a deterministic finite-difference approach is problematic in terms of the computation cost. A more efficient way is to solve Eq. (1) by a stochastic method. Here, a Lagrangian stochastic method [5] is used in which notional particles (Pope particles [49]) are populated into the flow field. Each particle can be loosely considered as a one-time realisation of the random turbulent motion of a fluid particle, undergoing simultaneous molecular mixing and chemical reaction processes.

In conventional (non-MMC like) models, the evolution of each particle can be recast into the following form:

$$\mathrm{d}x^*=[\mathbf{T}]\mathrm{d}t \quad (2)$$

$$\mathrm{d}\phi_k^*=[\mathbf{M}]\mathrm{d}t+[\mathbf{R}]\mathrm{d}t \quad (3)$$

In Eqs. (2) and (3), the superscript "$*$" denotes the quantities owned by the particles. Equation (2) represents particle transport in physical space denoted by the operator [**T**], which models the turbulent motion of fluid particles. Equation (3) represents the transport in composition space by the mixing operator [**M**] and reaction operator [**R**], which model the molecular mixing and chemical reaction, respectively. In principle, the operators [**T**], [**M**] and [**R**] should be devised in a way such that the statistics of particles yield a consistent PDF with Eq. (1). In the following context, the focus is put on [**T**] and [**M**].

2.1.2. Physical transport operator [T]

For the physical transport operator [**T**] in composition PDF methods, the gradient diffusion hypothesis is usually invoked [7]:

$$\mathrm{d}x^*=[\mathbf{T}]\mathrm{d}t=\left(\widetilde{u}+\frac{1}{\langle\rho\rangle}\frac{\partial\langle\rho\rangle\widetilde{\Gamma}_{\rm T}}{\partial x_j}\right)\mathrm{d}t+\sqrt{2\widetilde{\Gamma}_{\rm T}}\mathrm{d}W \quad (4)$$

where $\widetilde{\Gamma}_{\rm T}$ denotes the turbulent diffusivity. The transport operator includes a deterministic part, $\widetilde{u}+\nabla\left(\langle\rho\rangle\widetilde{\Gamma}_{\rm T}\right)/\langle\rho\rangle$, and a stochastic part, $\sqrt{2\widetilde{\Gamma}_{\rm T}}\mathrm{d}W$. The deterministic part represents the effects of the mean velocity field $\widetilde{u}$ and the turbulent diffusion, as modelled by the gradient diffusion hypothesis. The stochastic part includes increments of a Wiener process $\mathrm{d}W$ that models the transport as a random walk with step-size proportional to the square root of $\widetilde{\Gamma}_{\rm T}$. It should be noted that the transport operator in Eq. (4) represents the typical formulation in the TPDF framework and is also used in the SMMC and SPMM models. However, the OMMC model uses an alternative formulation introduced in Section 2.1.3. It should also be noted that the molecular transport in physical space is neglected in the present work, however it may be important under

some circumstances, i.e., prediction of carbon monoxide [50] at the base of the Cabra flame [51] (a lifted, turbulent partially-premixed methane/air flame).

To close Eq. (4), $\widetilde{\Gamma}_{\mathrm{T},i}$ requires modelling. In most studies, this is closed with input from a separate turbulence model. In the present study, however, $\widetilde{\Gamma}_{\mathrm{T},i}$ is extracted in such a way that it leads to the correct turbulent scalar fluxes for a selected scalar ϕ and thus that the transport of $\widetilde{\phi}$ is correctly reproduced. This can be achieved by considering the gradient hypothesis [7]

$$\langle\rho\rangle\langle u_i''|\underline{\psi}\rangle\widetilde{f}_\phi = -\widetilde{\Gamma}_{\mathrm{T},i}\frac{\partial\widetilde{f}_\phi}{\partial x_i} \tag{5}$$

With the model given by Eq. (5), all moments of any scalar have the same turbulent diffusivity, and as a result the turbulent diffusivity can be calculated from any scalar as

$$\widetilde{\Gamma}_{\mathrm{T},j} = -\frac{\widetilde{u_j''\phi''}}{\partial\widetilde{\phi}/\partial x_j} \tag{6}$$

where the r.h.s. of Eq. (6) can be calculated from DNS. In the present work considering nonpremixed flames it is calculated using Bilger's mixture fraction as the scalar, but in principle other scalars could be used, e.g., a progress variable as in [52,53].

2.1.3. Mixing operators [M]

In this work, conventional PDF approaches are represented by the mixing models IEM and EMST, representing extremes of models in which mixing is not local at all (IEM) and in which mixing is highly local (EMST).

In the conventional IEM mixing model, the molecular mixing term (the second term on the r.h.s. of Eq. (1)) is modelled as [7]:

$$\frac{\mathrm{d}\phi^*_{k,\mathrm{mix}}}{\mathrm{d}t} = -\frac{1}{2\tau_\phi}(\phi^*_k - \widetilde{\phi}_k), \tag{7}$$

where τ_ϕ denotes the scalar mixing time scale and its inverse $\Omega_\phi = 1/\tau_\phi$ is the scalar mixing frequency. Modelling of τ_ϕ is discussed later. Since the particle only interacts with the cell mean, the localness of IEM is restricted to the Reynolds-average level (assuming the computational grid is fine enough to resolve the Reynolds-averaged fields well). IEM also has some other undesirable properties, such as preserving the initial shape of the PDF, and hence not decaying eventually to a Gaussian distribution as expected.

To alleviate some of IEM's disadvantages, Subramaniam and Pope [21] proposed the EMST model. In EMST, a Euclidean minimum spanning tree is constructed in a high dimensional composition space [21]. After constructing the tree, particles are mixed pairwise with their neighbour(s) on the tree. In this sense, EMST is a fully local mixing model. However, the EMST violates independence and linearity of mixing. It can be also prone to so-called stranding wherein lower dimensional structures form in the composition space and particles tend to be attracted to them. To alleviate this, the EMST formulation incorporates an age parameter, which is a method that reduces the stranding effect somewhat by selecting a sub-set of particles for mixing each timestep; however in practice, EMST still often generates solutions that lie on low-dimensional manifolds [21,26].

In the present work, EMST is implemented according to the source code made available by Zhuyin Ren and Stephen Pope [54].

Both IEM and EMST, and the models to be introduced next, require the input of a user-specified mixing timescale τ_ϕ. Most TPDF mixing models assume that τ_ϕ is proportional to the turbulent time scale τ, i.e., $\tau = C_\phi\tau_\phi$, where the coefficient C_ϕ denotes the ratio of the scalar-to-turbulent mixing time scale. Hence the IEM model can be also expressed as

$$\frac{\mathrm{d}\phi^*_{k,\mathrm{mix}}}{\mathrm{d}t} = -\frac{C_\phi}{2\tau}(\phi^*_k - \widetilde{\phi}_k) \tag{8}$$

In a full *a posteriori* simulation, τ needs to be modelled. For example, the $k-\epsilon$ model [55] has been widely used for RANS simulations, in which τ is modelled as $\tau = k/\epsilon$, where k is the turbulent kinetic energy and ϵ is the turbulent dissipation rate. The turbulent kinetic energy can be also computed given a model, e.g., based on eddy viscosity concept, for Reynolds stress in RANS [56] or subgrid stress in LES context [57]. The value of C_ϕ is also needed to specify the unconditional mixing rate. It should be noted that C_ϕ is not universal but flow dependent and typically varying in the range of 1.5–8.0 [7,58].

Hence, the modelling of τ and C_ϕ introduces some uncertainties which make attribution of any discrepancies difficult to ascribe definitively to the mixing model. In the present work, these difficulties are circumvented since the mixing frequency Ω_ϕ is extracted directly from the DNS in order to correctly reproduce the dissipation of the variance of a selected scalar. Specifically, Ω_ϕ was calculated from the DNS as

$$\Omega_\phi = \widetilde{\chi}_\phi/\widetilde{\phi''^2} \tag{9}$$

where $\widetilde{\phi''^2}$ and $\widetilde{\chi}$ are the scalar dissipation rate and Favre-averaged variance, respectively, of the selected scalar. In the present work, as will be elaborated later, the Bilger mixture-fraction is used as the representative scalar.

2.2. MMC-like models

In MMC-like models, the Lagrangian particles are additionally ascribed one or more reference variables, and Eqs. (2) and (3) are complemented by one or more stochastic differential equations (SDEs) governing the evolution of the reference variable. In this work, the case of a single reference variable is considered, and the models considered all have the general form:

$$\mathrm{d}\Xi^* = A\mathrm{d}t + B\mathrm{d}W, \tag{10}$$

where Ξ^* is the reference variable, A is the drift coefficient, B is the diffusion coefficient, and $\mathrm{d}W$ is the increment of a Wiener process. The various models take different approaches to specifying A and B, which will be outlined later.

The key feature of the MMC-like models considered here is that the mixing is conditioned upon the reference scalar. Different mixing operators are possible, but to illustrate this, contrast the conventional IEM model (Eq. (7)) with the conditional IEM model:

$$\frac{\mathrm{d}\phi^*_{k,\mathrm{mix}}}{\mathrm{d}t} = -\frac{C_{\min}}{\tau}(\phi^*_k - \widetilde{\phi_k|\Xi}) \tag{11}$$

That is, the composition scalars ϕ^*_k are mixed towards their means $\widetilde{\phi_k|\Xi}$ *conditioned on the reference variable* Ξ. Here Ξ is a general representation of the reference variables used by different MMC-like models.

The main differences between each MMC-like mixing model lie in the selection and evolution of the reference variable, i.e., the form taken by the SDE (10). These are outlined in the following subsections.

2.2.1. OMMC model

The OMMC model used here is a stochastic implementation of MMC following that in [10,28,35]. A unit Gaussian reference variable, ζ, is related to the mixture fraction Z by the mapping function Z_ζ. Instead of using the conventional form of physical transport operator [**T**] in Eq. (4), the OMMC model employs a different closure for turbulent diffusion transport. The model is constructed, however, so that it results in gradient transport of the mean mixture fraction. The particle position x^* and reference variable ζ^* evolve as follows, respectively:

$$\mathrm{d}x^* = (\widetilde{u} + u^{(1)}\zeta^*)\mathrm{d}t \tag{12}$$

$$\mathrm{d}\zeta^* = A^0\mathrm{d}t + b^0\mathrm{d}W_\zeta \tag{13}$$

The minor mixing of ϕ_k and Z_ζ are performed in a similar way as Eq. (11), that is:

$$\mathrm{d}\phi^*_{k,\mathrm{mix}} = -\frac{C_{\min}}{\tau}\left(\phi^*_k - \widetilde{\phi|\zeta}\right)\mathrm{d}t \tag{14}$$

$$\mathrm{d}Z^*_\zeta = -\frac{C_{\min}}{\tau}\left(Z^*_\zeta - \widetilde{Z_\zeta|\zeta}\right)\mathrm{d}t \tag{15}$$

In Eqs. (12) and 13, $\mathrm{d}W_\zeta$ is a Wiener process for ζ; $\widetilde{u}$ is the Favre mean velocity; $u^{(1)}\zeta^*$ is the model for the turbulent diffusion. The coefficients $u^{(1)}$, A^0, and b^0 are given in the following forms [20]:

$$u^{(1)} = \frac{\widetilde{u''Z''_\zeta}}{\langle\zeta Z_\zeta\rangle}, \tag{16}$$

$$A^0 = -B\zeta^* + \frac{1}{\langle\rho\rangle}\nabla\cdot(\langle\rho\rangle u^{(1)}), \tag{17}$$

$$b^0 = \sqrt{2B}, \tag{18}$$

$$B = \frac{\widetilde{\chi}(Z_\zeta)}{2}\left\langle\left(\frac{\partial Z_\zeta}{\partial\zeta}\right)^2\right\rangle^{-1} \tag{19}$$

The term $\partial Z_\zeta/\partial\zeta$ is approximated by $\partial\langle Z_\zeta|\zeta\rangle/\partial\zeta$. For $u^{(1)}$, the gradient transport hypothesis is again invoked [10,20,28,35]:

$$u^{(1)} = \frac{\widetilde{u''Z''_\zeta}}{\langle\zeta' Z'_\zeta\rangle} = -\frac{\widetilde{\Gamma}_\mathrm{T}\nabla\widetilde{Z}_\zeta}{\langle\zeta' Z'_\zeta\rangle} \tag{20}$$

The scalar dissipation term $\widetilde{\chi}(Z_\zeta)$ in Eq. (19) is modelled using Corrsin's model [59] as:

$$\widetilde{\chi}(Z_\zeta) = \frac{C_\phi}{\tau}\widetilde{Z''^2_\zeta} \tag{21}$$

where C_ϕ/τ is unconditional scalar mixing frequency and its definition is consistent with that in Eq. (7). In the OMMC model, the coefficient $C_{\min}$ needs to be specified.

2.2.2. SPMM

In the SPMM model, the physical transport operator [**T**] is modelled by Eq. (4). The shadow displacement, R, is used as the reference variable [8]. The variable R represents the displacement between the shadow position, which can be considered as an inseparable companion of the fluid particle with random distance, and the real fluid particle position. The shadow displacement R is obtained from the following transport equation:

$$\mathrm{d}R^* = -\frac{a}{\tau}R^*\mathrm{d}t + b\sqrt{2\widetilde{\Gamma}_\mathrm{T}}\mathrm{d}W_R \tag{22}$$

In the Eq. (22), the coefficient a controls the drift of R; b controls the random walk; $\mathrm{d}W_R$ are increments of a Wiener process for R, which are independent from $\mathrm{d}W$ in Eq. (4). The minor mixing operator for the composition scalars is then given by a relaxation to their means conditioned on R:

$$\mathrm{d}\phi^*_{k,\mathrm{mix}} = -\frac{C_{\min}}{\tau}\left(\phi^*_k - \widetilde{\phi|R}\right)\mathrm{d}t \tag{23}$$

In the present work, b is set to zero following a suggestion made in Ref. [8]. Hence the coefficients a and $C_{\min}$ are all that remain to be specified.

2.2.3. SMMC model

Analoguous to the SPMM model, the physical transport operator [**T**] in the SMMC is modelled by Eq. (4). The reference variable, ξ, is introduced to mimic the behaviour of mixture fraction Z. That is, ξ is devised such that it has approximately the same mean and variance as mixture fraction Z. The reference variable ξ is evolved by an Ornstein–Uhlenbeck process [40]:

$$\mathrm{d}\xi^* = -\frac{C_\xi}{\tau}(\xi^* - \tilde{\xi})\mathrm{d}t + b_0\sqrt{\frac{2C_\xi\widetilde{\xi''^2}}{\tau}}\mathrm{d}W_\xi \tag{24}$$

In Eq. (24), the coefficient C_ξ controls the drift of ξ towards its unconditional mean; C_ξ controls the random walk and $\mathrm{d}W_\xi$ is a Wiener process of ξ, independent of $\mathrm{d}W$ in Eq. (4). The composition scalars are mixed towards their conditional means, conditioned on the reference variable ξ:

$$\mathrm{d}\phi^*_{k,\mathrm{mix}} = -\frac{C_{\min}}{\tau}\left(\phi^*_k - \widetilde{\phi|\xi}\right)\mathrm{d}t \tag{25}$$

In the SMMC model, the coefficients C_ξ, b_0 and $C_{\min}$ need to be specified.

2.2.4. MMC-like models summary

Key similarities and differences about each MMC-like mixing models are summarised in Table 1. For the physical transport operator, Eqs. (4) and (12) produce a similar outcome in that they both model the stochastic particle location x^*_i leading to gradient transport of the mean mixture fraction. The difference in approach is that Eq. (4) directly imposes the model for x^*_i without needing the particle velocity to be computed, whereas Eq. (12) uses the velocity model implied by Eq. (20). For the scalar mixing, the major mixing operator models the evolution of reference variable. The minor mixing models all have an identical form that relaxes to the conditional mean, but differs in the conditioning reference variable, Ξ, as listed in the "Reference variable" row. More details of each model can be found in Refs. [10,20,28] for the OMMC model, Refs. [8,45] for the SPMM model and Refs. [40,41] for the SMMC model.

2.3. Specification of the coefficients for MMC-like mixing models

Specification of the model coefficients in stochastic MMC-like models is more difficult than in conventional PDF methods since the behaviour of the reference variable SDE has to be considered together with the PDF equations. In this work, the method proposed in Ref. [40] for the coefficient specification of the SMMC model is used and extended for specifying the OMMC and SPMM model coefficients. In the present work, two outcomes for the specification of the coefficients are desired [40]:

1. The molecular dissipation rate of a passive scalar ϕ should be physically correct, which has been determined by theory and demonstrated by DNS studies [59] to be well approximated by:

$$\frac{\mathrm{d}\widetilde{\phi''^2}}{\mathrm{d}t} = -\frac{C_\phi}{\tau}\widetilde{\phi''^2} \tag{26}$$

2. The model localness should be controllable by the user; here we take it to be measured by the correlation coefficient between the scalar ϕ and reference variable Ξ, which is denoted as:

$$r = \frac{\widetilde{\Xi'\phi'}}{\sqrt{\widetilde{\Xi'^2}}\sqrt{\widetilde{\phi'^2}}} \tag{27}$$

It is challenging to achieve the above two outcomes in general flows. However, in certain simple configurations, and after modelling transport and the mixing timescale, model outcomes are analytic, and coefficient settings can be determined by imposing the above two principles.

Table 1
Summary of the MMC-like molecular mixing models.

	OMMC	SPMM	SMMC
Physical transport	$dx^* = (\tilde{u} + u^{(1)}\zeta^*)dt$	$dx^* = (\tilde{u} + \frac{1}{\langle\rho\rangle}\frac{\partial\langle\rho\rangle\tilde{\Gamma}_T}{\partial x}dt) + \sqrt{2\tilde{\Gamma}_T}dW$	
Scalar transport	$d\phi_k^* = d\phi_{k,mix}^* + d\phi_{k,react}^*$		
Major mixing	$d\zeta^* = A^0dt + b^0dW_\zeta$	$dR^* = -\frac{a}{\tau}R^*dt + b\sqrt{2\tilde{\Gamma}_T}dW_R$	$d\xi^* = -\frac{C_\xi}{\tau}(\xi^* - \tilde{\xi})dt + b_0\sqrt{\frac{2C_\xi\widetilde{\xi'^2}}{\tau}}dW_\xi$
Minor mixing	$d\phi_{k,mix}^* = -\frac{C_{\min}}{\tau}\left(\phi_k^* - \widetilde{\phi_k\|\zeta}\right)dt$	$d\phi_{k,mix}^* = -\frac{C_{\min}}{\tau}\left(\phi_k^* - \widetilde{\phi_k\|R}\right)dt$	$d\phi_{k,mix}^* = -\frac{C_{\min}}{\tau}\left(\phi_k^* - \widetilde{\phi_k\|\xi}\right)dt$
Reference variable	ζ: can be designed to mimic any real physical variable	R: shadow displacement moving jointly with fluid particle	ξ: statistically equal to real mixture fraction

Table 2
Analytical solution of scalar variances and covariance of the three MMC-like mixing models in MSG flow.

	OMMC	SPMM	SMMC
Reference variable $\widetilde{\Xi'^2}$	$\frac{d\widetilde{\zeta'^2}}{dt} = -\frac{C_\phi}{\tau r^2}\left(\widetilde{\zeta'^2}\right)^2 + \frac{C_\phi\widetilde{\zeta'^2}}{\tau r^2}$	$\frac{d\widetilde{R'^2}}{dt} = -\frac{2a}{\tau}\widetilde{R'^2} + [2\Gamma_T(b^2+1)]$	$\frac{d\widetilde{\xi'^2}}{dt} = 2G^2\Gamma_T - \frac{2C_\xi(1-b_0^2)}{\tau}\widetilde{\xi'^2}$
Scalar $\widetilde{\phi'^2}$	$\frac{d\widetilde{\phi'^2}}{dt} = 2G^2\Gamma_T - \frac{2C_{\min}}{\tau}\widetilde{\phi'^2}(1-r^2)$	$\frac{d\widetilde{\phi'^2}}{dt} = 2G^2\Gamma_T - \frac{2C_{\min}}{\tau}\widetilde{\phi'^2}(1-r^2)$	$\frac{d\widetilde{\phi'^2}}{dt} = 2G^2\Gamma_T - \frac{2C_{\min}}{\tau}\widetilde{\phi'^2}(1-r^2)$
Covariance $\widetilde{\Xi'\phi'}$	$\frac{d\widetilde{\phi'\zeta'}}{dt} = -\frac{C_\phi}{2\tau r^2}\widetilde{\phi'\zeta'}\widetilde{\zeta'^2} + G^2\Gamma_T\frac{\widetilde{\zeta'^2}}{\widetilde{\zeta'\phi'}}$	$\frac{d\widetilde{R'\phi'}}{dt} = 2G\Gamma_T - \frac{a}{\tau}\widetilde{R'\phi'}$	$\frac{d\widetilde{\xi'\phi'}}{dt} = 2G^2\Gamma_T - \frac{C_\xi}{\tau}\widetilde{\xi'\phi'}$

In the present work, a canonical flow configuration with a mean scalar gradient (MSG) is used to specify the coefficients. The MSG flow is essentially a homogeneous, statistically stationary turbulent flow field characterised by the turbulent diffusivity Γ_T and the turbulent mixing time scale τ. The mean scalar has a uniform gradient, denoted as $G = \partial\tilde{\phi}/\partial x$ where x is the spatial coordinate. In a MSG flow, the temporal evolution of $\widetilde{\phi'^2}$, $\widetilde{\Xi'^2}$ and their covariances, $\widetilde{\phi'\Xi'}$, can be obtained analytically; the results for each model are presented in Table 2. Here, the SMMC model is taken as an illustrative example ($\Xi = \xi$). Similar procedures can be followed to specify the other two MMC-like mixing models.

For the SMMC model in the MSG flow, $\widetilde{\xi'^2}$, $\widetilde{\phi'^2}$ and $\widetilde{\phi'\xi'}$ analytically evolve as follows [40]:

$$\frac{d\widetilde{\xi'^2}}{dt} = \mathcal{P} - \frac{2C_\xi(1-b_0^2)}{\tau}\widetilde{\xi'^2} \tag{28}$$

$$\frac{d\widetilde{\phi'^2}}{dt} = \mathcal{P} - \frac{2C_{min}}{\tau}\widetilde{\phi'^2}(1-r^2) \tag{29}$$

$$\frac{d\widetilde{\xi'\phi'}}{dt} = \mathcal{P} - \frac{C_\xi}{\tau}\widetilde{\xi'\phi'} \tag{30}$$

The above equation sets reveal that the evolution of variances in MSG flow is contributed by two parts: the turbulent production of variances caused by the scalar gradient, $\mathcal{P} = 2G^2\Gamma_T$, and the homogeneous decay part (the second term on the r.h.s of each above equation). At steady state limit when $d(\cdot)/dt$=0, $\widetilde{\xi'^2}$, $\widetilde{\phi'^2}$ and $\widetilde{\phi'\xi'}$ have the following fixed points (denoted with a subscript "s"):

$$\widetilde{\xi_s'^2} = \mathcal{P}\tau/C_\phi \tag{31}$$

$$\widetilde{\phi_s'^2} = \mathcal{P}\tau/C_\phi \tag{32}$$

$$\widetilde{\phi_s'\xi_s'} = \mathcal{P}\tau/C_\xi \tag{33}$$

In the MSG flow, $\widetilde{\xi'^2}$, $\widetilde{\phi'^2}$ and $\widetilde{\xi'\phi'}$ always approach their steady state values, and the corresponding correlation coefficient at steady state, r_t, is referred to as the "target correlation coefficient":

$$r_t = \frac{\widetilde{\phi_s'\xi_s'}}{\sqrt{\widetilde{\xi_s'^2}}\sqrt{\widetilde{\phi_s'^2}}} \tag{34}$$

Applying Principle 1 by equating the homogeneous decay part of $\widetilde{\xi'^2}$ and $\widetilde{\phi'^2}$ to the desired model in Eq. (26) yields:

$$C_\phi = 2C_\xi\left(1 - b_0^2\right) \tag{35}$$

$$C_\phi = 2C_{min}\left(1 - r_t^2\right) \tag{36}$$

Applying Principle 2 yields:

$$r_t = \frac{C_\phi}{C_\xi} \tag{37}$$

Combining Eqs. (35), (36) and (37), the SMMC coefficients can be expressed as a function of r_t as:

$$C_\xi = C_\phi/r_t, \quad C_{min} = \frac{C_\phi}{2(1-r_t^2)}, \quad b_0 = \sqrt{1 - \frac{r_t}{2}}, \tag{38}$$

where C_ϕ and r_t are model input parameters, which control the unconditional dissipation rate and model localness, respectively.

The MMC-like models by definition are local in reference variable space, but physically it is expected that mixing be local in composition space (and physical space). For instance in the SMMC model, it is desired that the localness in ξ-space naturally results in the localness in ϕ-space. This linkage is achieved by r_t, such that a higher correlation suppresses minor fluctuations and subsequently leads to a high level of localness. In a full *a posteriori* simulation, C_ϕ and r_t both need to be prescribed to specify the unconditional dissipation rate and the model localness, respectively. As mentioned above, in the present work, the mixing frequency C_ϕ/τ is obtained from the DNS. Only r_t is a free parameter which is used to investigate the effects of localness. It needs to be provided by the user since it is obviously not available in DNS. In the present work, three values, $r_t = 0.5, 0.7$ and 0.9 are selected to represent a low, intermediate and high level of localness, respectively.

In this work, a similar procedure has been followed to specify the OMMC and SPMM model coefficients. The detailed derivations are presented in Appendix A. The coefficients of the OMMC, SPMM and SMMC models are summarised in Table 3.

2.4. Numerical approach

The numerical approach used in the present work follows that described in Ref. [26]. Three DNS datasets (referred to as Case 1, 2, 3) of turbulent nonpremixed ethylene flames [3] with decreasing Damköhler (Da) numbers and thus increasing extinction levels are

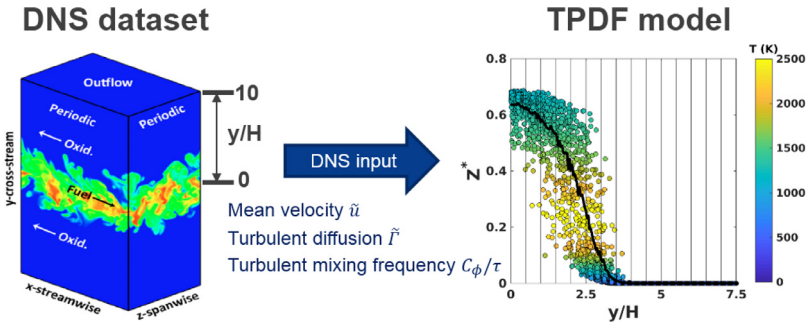

Fig. 1. Schematic plot of the work flow. On the left is the DNS configuration of the ethylene nonpremixed flame reproduced from Ref. [3]. On the right is the scatter plot of mixture fraction versus the physical location of the PDF particles along the cross-stream direction. The black solid line indicates the mean mixture fraction $\langle Z \rangle$. Vertical lines indicate the finite volume grid and the particles are coloured by the instantaneous temperature.

Table 3
Cofficients of the three MMC-like models specified by the MSG flow.

OMMC	SPMM	SMMC
$C_{\min} = \frac{C_\phi}{2(1-r_t^2)}$	$C_{\min} = \frac{C_\phi}{2(1-r_t^2)}$	$C_{\min} = \frac{C_\phi}{2(1-r_t^2)}$
	$a = \frac{2C_\phi}{r_t^2(1+b^2)}$	$C_\xi = \frac{C_\phi}{r_t}$
	$b = 0$ suggested by [8]	$b_0 = \sqrt{1-\frac{r_t}{2}}$

Table 4
Several characteristic parameters of Case 1-3.

	Case 1	Case 2	Case 3
Damköhler number (Da)	0.023	0.017	0.011
Extinction scalar dissipation rate χ_q [1/s]	4774	2580	2380
Reynolds number (Re)	5120	5120	5120
Fuel/air velocity difference ΔU [m/s]	196	196	196
Velocity core height H [mm]	0.96	0.96	0.96

used for validation. All three cases undergo first extinction due to the strong mixing and then reignition as mixing rates relax.

The DNS configuration is essentially a temporally evolving plane-jet flame (Fig. 1). A three-dimensional planar slab of fuel is surrounded by two counter-flowing oxidiser streams with a velocity difference $\Delta U = 196 m/s$. The characteristic jet time is defined as $t_j = H/\Delta U$ where H denotes the characteristic fuel jet height. The flame was initialised from a steady flamelet solution. The extinction level of the turbulent jet flame was controlled by Da, which was defined as $Da = \chi_q t_j$. The stoichiometric extinction scalar dissipation rate, χ_q, was varied by adjusting the nitrogen concentration of the fuel and oxidiser streams. This results in $Da = 0.023, 0.017$ and 0.011 for Case 1–3, respectively. The Case 1 and 3 experiences the least and most extinction, respectively. The Case 2 reignites but is close to the edge of extinction. The initial profile of mean mixture fraction, $\langle Z \rangle_{\mathrm{DNS}}$, varies only along the transverse direction, denoted as y. The DNS configuration allows averaging along the streamwise (x) and spanwise (z) direction, leaving statistics dependent only upon y and time t. Hence the computational domain used for TPDF simulation is spatially one-dimensional. In the current work, y and t are normalised by the characteristic jet height ($H = 0.96$ mm) and the characteristic jet time ($t_j = 0.0049$ ms) [3]. Due to the symmetry along y direction, the comparison can be performed within the range $0 \le y/H \le 10$ (Table 4).

As mentioned above, the TPDF approach requires a turbulence closure. In the current work, the turbulent flow field information is directly extracted from the DNS, including the mean velocity field $\widetilde{u}$, the turbulent diffusivity $\widetilde{\Gamma}_{\mathrm{T}}$ and the mixing frequency C_ϕ/τ. This approach allows elimination of uncertainties due to the turbulence modelling. Here the mixture fraction Z is used as the target scalar in Eqs. (6) and (9). Specifically, from the DNS, the turbulent diffusivity is calculated as $\widetilde{\Gamma}_{\mathrm{T}} = -(\langle \rho u Z \rangle - \overline{\rho}\widetilde{u}\widetilde{Z})/\overline{\rho}\nabla\widetilde{Z}$ where $\widetilde{Z}$ is the Favre-mean mixture fraction. The mixing frequency $\Omega_\phi = C_\phi/\tau$ is calculated as $\Omega_\phi = 2\mathcal{D}_T|\widetilde{\nabla Z}|^2/\widetilde{Z''^2}$ where $\mathcal{D}_T$ is the thermal diffusivity. All Favre-mean fields are first calculated by ensemble averaging along x and z directions (Fig. 1) and statistical noise is removed along the y direction by a spline smoothing function. The present work adopts a Matlab implementation [60] of the cubic smoothing algorithm proposed in Ref. [61]. The level of smoothing is controlled by a parameter, $1-\epsilon$, such that increasing the small quantity ϵ leads to a higher level of smoothing. Most of the DNS input values, including mixing frequency and those for TPDF initialisation such as temperature and composition fields, are not sensitive to the smoothing level since good statistical convergence can be obtained from the DNS. The main difficulty comes from the smoothing of turbulent diffusivity $\widetilde{\Gamma}_{\mathrm{T}} = -\widetilde{u''Z''}/(\partial\widetilde{Z}/\partial y)$ at the centreline. In this region, both the turbulent scalar flux (nominator) and mean scalar variance (denominator) approach zero but the limit of their ratio should be non-zero and is unavailable from DNS. Here, the value of ϵ was tuned by trial-and-error to yield a correct $\widetilde{\Gamma}_{\mathrm{T}}$, such that the profile of $\widetilde{Z}$ was reproduced over the whole domain. These DNS inputs are stored in a lookup table on a well refined mesh (much finer than the TPDF grid) and the tabulated data is then linearly interpolated to the particle location during the TPDF simulation.

The MMC-like models are implemented in an in-house code which has been successfully used for TPDF simulations of turbulent nonpremixed flames [26,46], premixed flames [52,53] and spray flames [48]. Equations (2) and (3), along with the chemical reaction term are advanced by a symmetric Strang splitting scheme [62], which can be denoted as **TMRMT**. In this scheme the transport operator [**T**] and mixing operator [**M**] are performed twice per time step in a symmetric manner with respect to [**R**]. Without the Wiener term, the scheme yields second-order accuracy in time. The chemical reaction sub-step [**R**] is solved using a 6-stage, 4th order Runge–Kutta method [26], same as the one used by the DNS solver.

The conditional mean of scalars, $\widetilde{\phi|\Xi}$, is calculated in a similar way as in [8]. Specifically, particles in each mesh cell are first sorted in ascending order in Ξ-space. The conditional mean of the jth sorted particle, $\widetilde{\phi^j|\Xi}$, is approximated by the mean of its two nearest neighbour particles in Ξ-space, that is:

$$\widetilde{\phi^j|\Xi} = \frac{1}{2}(\phi^{j-1} + \phi^{j+1}) \tag{39}$$

The conditional mean of boundary particles in Ξ-space is approximated as:

$$\widetilde{\phi^1|\Xi} = \frac{1}{2}(\phi^1 + \phi^2) \tag{40}$$

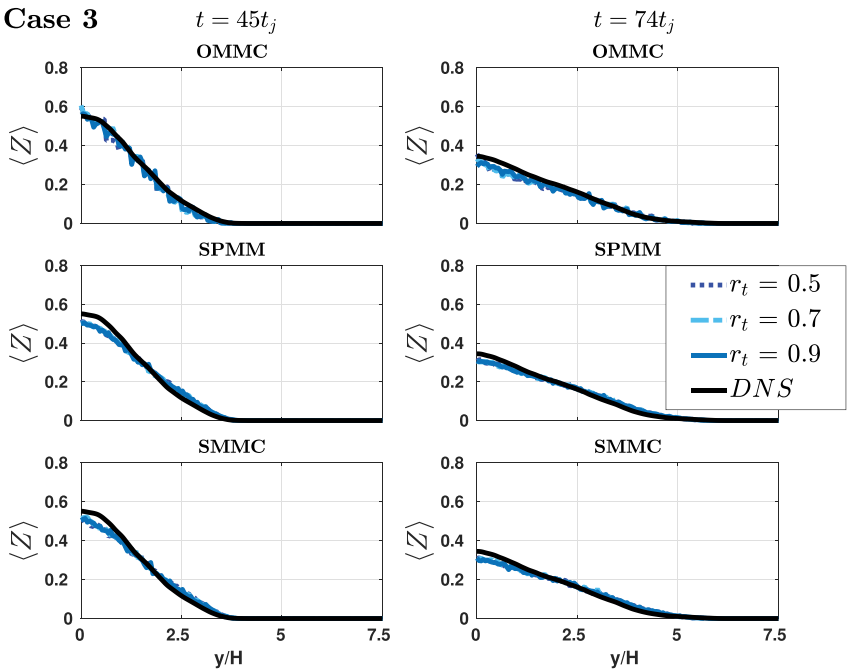

Fig. 2. Mean mixture fraction comparison for the OMMC (first row), SPMM (second row) and SMMC (third row) model for Case 3 with $r_t = 0.5, 0.7$ and 0.9 at 45 (left column) and 74 (right column) characteristic jet times.

$$\widetilde{\phi^{N_{pc}}|\Xi} = \frac{1}{2}(\phi^{N_{pc}} + \phi^{N_{pc}-1}) \tag{41}$$

The numerical implementation of the three MMC-like models is validated in simulations of a MSG flow for which an analytical solution can be obtained and the results are presented in Appendix B.

The MMC-like models are initialised as follows. First, the particles are evenly populated into the computational domain. Then the $\langle Z \rangle_{DNS}$ is spatially interpolated to PDF particles such that $\langle Z \rangle = \langle Z \rangle_{DNS}$. For the SMMC model, the reference variable ξ^* is initialised by setting $\xi^* = Z^*$. For the SPMM model, the shadow displacement R^* is initialised with a Gaussian distribution, with $\langle R \rangle = 0$ and $\langle R'^2 \rangle = \Delta y^2$ where Δy is the grid size.

For the OMMC model, Z^*_ζ, should be initialised equal to Z^* since Z^*_ζ is a model for the real mixture fraction. The reference variable ζ^* should always be a unit Gaussian. However, such strategy is problematic in the current work since the DNS starts from a laminar solution with zero variance. Consequently, $\langle Z'_\zeta \zeta' \rangle$ would be zero, which causes the $u^{(1)}$ term to diverge. To overcome this issue, we advance the simulation for the first 5 jet times with the SMMC model to generate an initial level of turbulent mixing and thus a non-zero profile of mixture fraction variance. Then the simulation is switched to continue with the OMMC model and Z^*_ζ is initialised as Gaussian with the mean and variance equal to those calculated from the SMMC model at $t = 5t_j$. The reference variable ζ^* is initialised in full correlation with Z^*_ζ as Gaussian, but with zero mean and unity variance. To avoid spurious oscillations, a minimum value 1×10^{-6} is enforced for $\langle Z'_\zeta \zeta' \rangle$, as was done in Refs. [28,35]. More details of the numerical implementation of the OMMC model can be found in Appendix C.

The key numerical parameters for the TPDF simulations are: the number of cells, $N_{cell} = 192$; the number of particles per cell, N_{pc}, is initialised as $N_{pc} = 500$; the time step, Δt, is 5 ns for Case 1, and 10 ns for Case 2 and 3. Convergence studies [26] showed these values are more than adequate for all the cases considered. It is not implied that such a high cell and particle number is actually required in a practical setting, we simply made these choices in order to eliminate stochastic or discretisation errors as a main cause of errors, allowing a clean focus on the mixing models.

3. Results and discussion

First, the results for the mean and RMS mixture fraction are presented in Section 3.1 to validate the mixing of an inert scalar. In Section 3.2, the MMC-like mixing models are evaluated in terms of the prediction of extinction and reignition events. In Section 3.3, the conditional statistics of the flame are examined.

3.1. Mixture fraction

Figure 2 shows the mean mixture fraction profile, $\langle Z \rangle$, for Case 3 at 45 and $74t_j$ as a function of the normalised spatial coordinate y/H. The results of Case 1 and 2 are qualitatively similar and thus not presented. It is shown that all three MMC-like mixing models yield only marginal differences compared to the DNS data. Such good agreement is expected since by construction, i.e., extracting turbulent flow information from the DNS, the prediction of the mean mixture fraction should not be affected by the choice of mixing model or the level of localness. Besides, this result also provides confidence that the numerical implementation of the TPDF method is consistent and correct.

Figure 3 shows the results of the mixture fraction RMS, Z_{rms}, for Case 3. All three mixing models adequately match the temporal evolution of Z_{rms}. The SMMC model yields the best agreement with the DNS for all three r_t values. The OMMC model also correctly predicts Z_{rms} but with a slight under-prediction observed. Both the SMMC and OMMC model show little dependence on r_t. The SPMM model underestimates Z_{rms} with increasing deviation with larger r_t.

In previous work [40,41], the SMMC model's parameters were set by matching the expected scalar variance decay in homogeneous isotropic turbulence (HIT). To make a comparison to the present settings based on the MSG flow, the results of Z_{rms} obtained from simulations with HIT coefficient set (referred to as

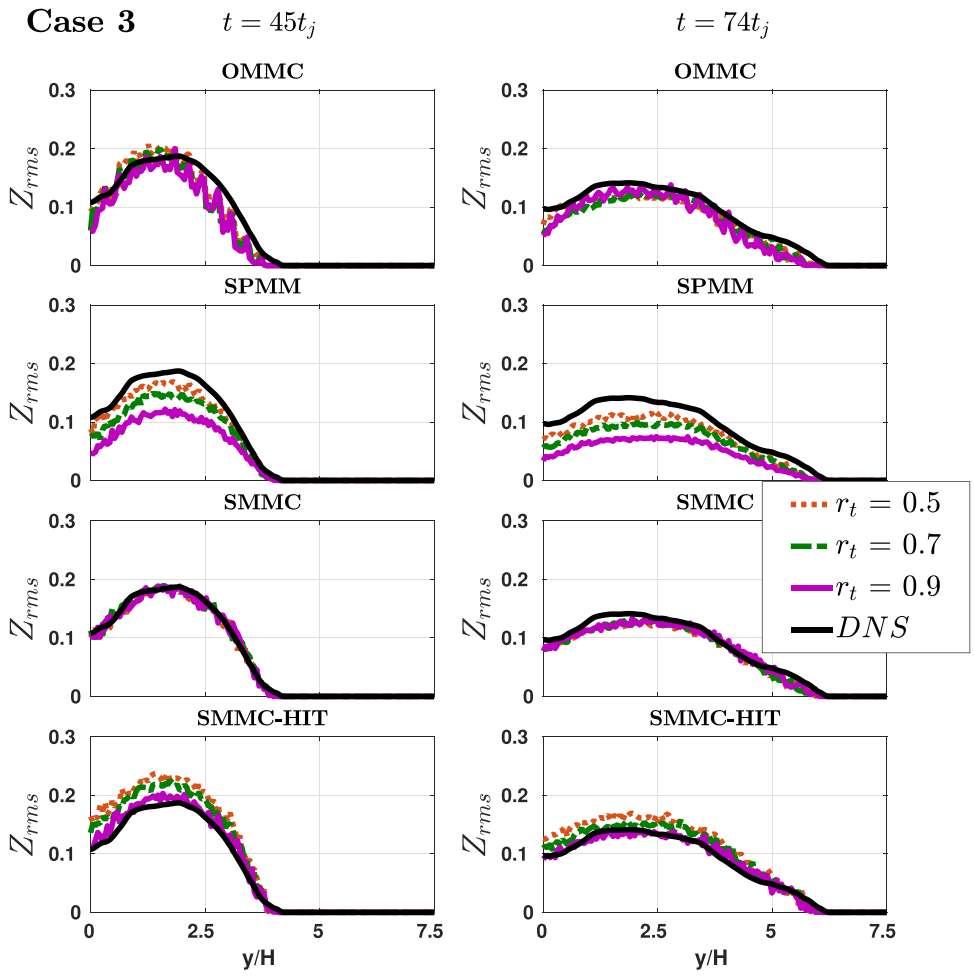

Fig. 3. RMS mixture fraction comparison for the OMMC (first row), SPMM (second row) and SMMC (third row) model for Case 3 with $r_t = 0.5$, 0.7 and 0.9 at 45 (left column) and 74 (right column) characteristic jet times. The results of the SMMC-HIT coefficient set are also presented (last row).

SMMC-HIT) are also presented in the last row of Fig. 3. This shows that the SMMC-HIT model over-predicts the Z_{rms} when the localness is relatively low ($r_t = 0.5, 0.7$) and only yields good agreement when $r_t = 0.9$, corresponding to a high level of localness. This is in contrast to the results with the SMMC-MSG model which agree well with the DNS for all the selected r_t values. This suggests an advantage of the MSG coefficient set over that from HIT: the SMMC model parameterised with coefficients obtained from the MSG flow configuration can change the model localness without adversely affecting the prediction of Z_{rms}. Such improvement can be attributed to the fact that the MSG flow takes into account the effect of a scalar gradient on the correlation between reference variable and mixture fraction.

3.2. Extinction and reignition

In this section, the MMC-like mixing models are examined in terms of the capability for predicting the overall extinction and reignition behaviour. This task is challenging because close to the point of extinction or reignition, small changes in mixing rates can cause large changes in the state of flame. Figures 4, 6 and 8 show contours of the mean temperature profile, $\langle T \rangle$, as a function of space (y) and time, as well as the evolution of the maximum mean temperature in the domain, $\langle T \rangle_{\max}$, for Case 1, 2 and 3, respectively. To provide a quantitative comparison, the profiles of mean and RMS temperature are presented for Case 1, 2 and 3 as shown in Figs. 5, 7 and 9, respectively. Two time instants are selected, $t = 45$ and $74t_j$, corresponding to the onset of reignition and the fully burning state. For Case 1 with the highest Damköhler number (lowest extinction level), the DNS shows that the flame goes through three distinct stages: (1) initial mixing dominated by laminar diffusion ($t < 5t_j$); (2) extinction due to the increasing intensity of turbulent dissipation ($5 < t_j < 15t_j$) and (3) reignition ($t_j > 15t_j$). When the level of localness is low ($r_t = 0.5$), both the SPMM and SMMC models overpredict the extinction with no sign of reignition, while the OMMC model predicts the reignition but at a later stage (around $t = 60t_j$) compared to the DNS. As the localness increases to an intermediate level ($r_t = 0.7$), all three MMC-like mixing models predict stronger reignition. The OMMC model predicts consistent reignition timing with the DNS while the SPMM and SMMC model predict a later reignition around $t = 50t_j$. When the level of localness is high ($r_t = 0.9$), all three MMC-like mixing models predict correctly the occurrence of the extinction and reignition. Also of note, $\langle T \rangle_{\max}$ is over-predicted initially by all mixing models which can be mainly attributed to the fact that the current TPDF method does not account for the laminar transport effect.

The effect of localness can be further investigated by comparison with results obtained with the IEM and EMST models, both of which have been implemented and validated in previous work [26]. It is seen that the IEM model predicts no reignition. Since many very thin reaction zones would physically exist in each TPDF grid cell, localness is required to resolve the sub-cell process. As indicated by Eq. (7), in the IEM model all the scalars are mixed by relaxation towards their unconditional means and thus ade-

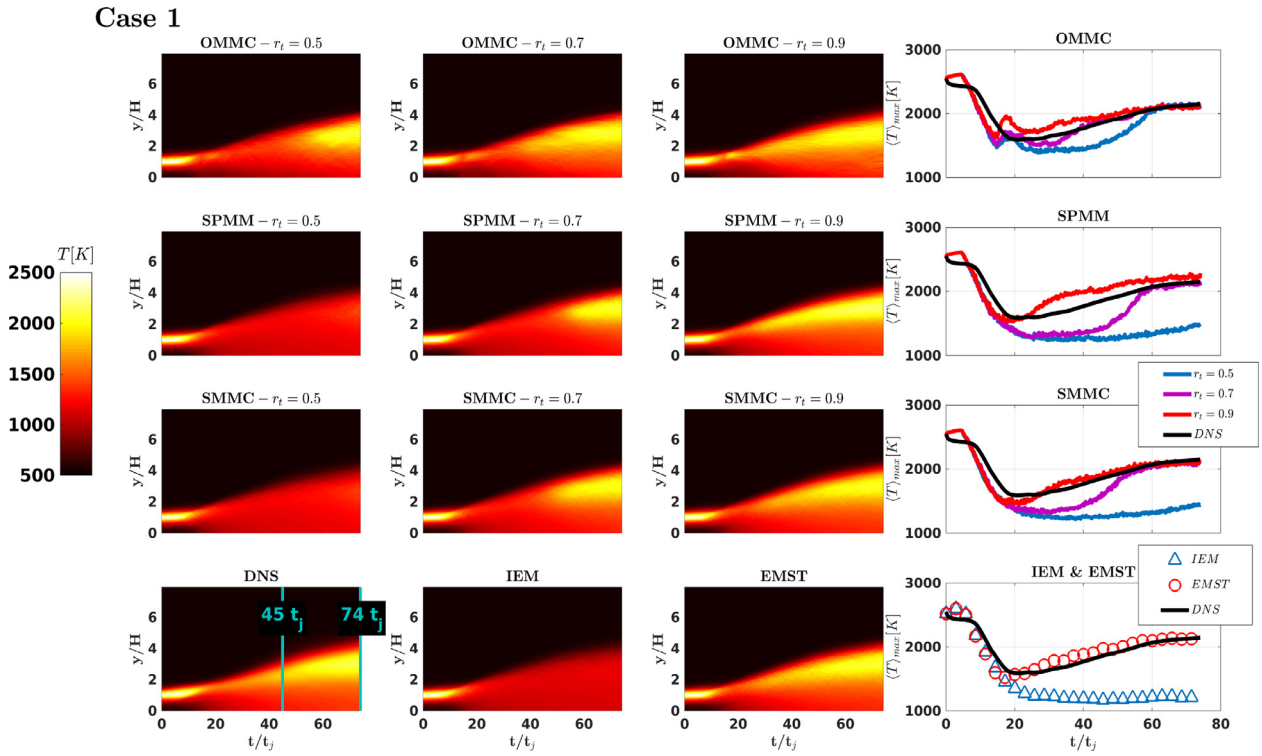

Fig. 4. Extinction and reignition events for Case 1. On the left is the contour coloured by mean temperature for the OMMC (first row), SPMM (second row) and SMMC (third row) model. On the right is the corresponding evolution of the maximum mean temperature in the domain. The results of the DNS, IEM model and EMST model (last row) are also shown for reference.

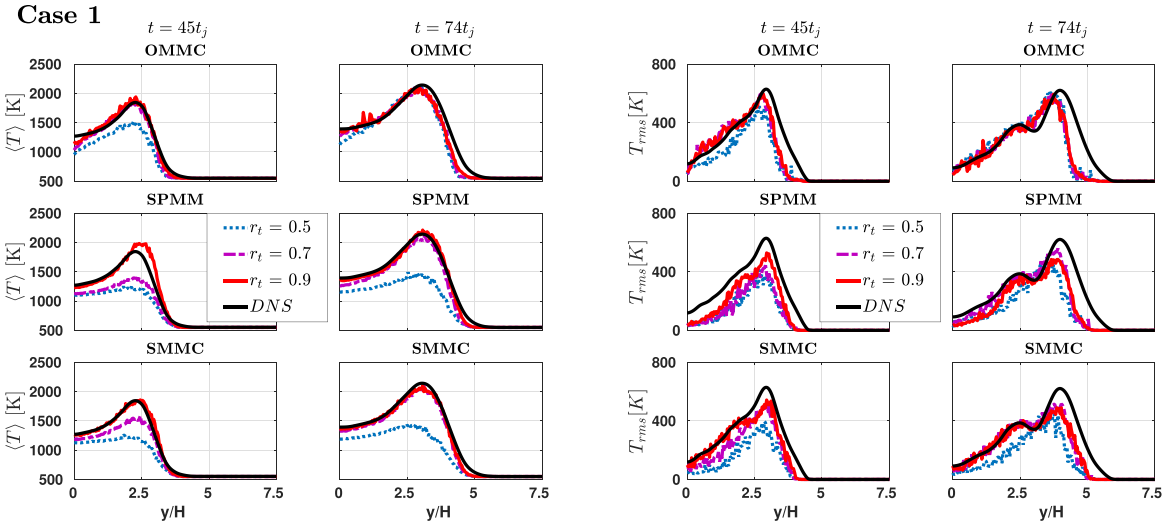

Fig. 5. Mean (left) and RMS (right) temperature comparison for the OMMC (first row), SPMM (second row) and SMMC (third row) model for Case 1 with $r_t = 0.5$, 0.7 and 0.9 at 45 and 74 characteristic jet times.

quate localness is not provided, leading to unphysical extinction. In contrast, the EMST model correctly predicts the reignition since it can ensure localness by mixing with particles close in composition space. For the SPMM and SMMC models, the result of $r_t = 0.5$ resembles that of the IEM model, and the result of $r_t = 0.9$ resembles that of the EMST model.

Figure 5 shows the mean and RMS temperature profile at 45 and $74t_j$ for Case 1. For $\langle T \rangle$, $r_t = 0.9$ yields quantitatively good agreement with the DNS. The results of T_{rms} also agrees reasonably well with the DNS as the occurrence of extinction and reignition is predicted. However, when the flame is fully ignited ($t = 74t_j$), the MMC-like mixing models tend to underestimate T_{rms} at the edge of the jet.

For Case 2 with an increased level of extinction (Fig. 6), both low ($r_t = 0.5$) and intermediate ($r_t = 0.7$) levels of localness predict no reignition for all three MMC-like mixing models. When $r_t = 0.9$, all three MMC-like mixing models along with the EMST model predict extinction and reignition correctly. The IEM model fails to predict any reignition due to the lack of localness. Again, the MMC-like models with $r_t = 0.9$ yield results similar to those obtained with the EMST model and $r_t = 0.5$ similar to the IEM model.

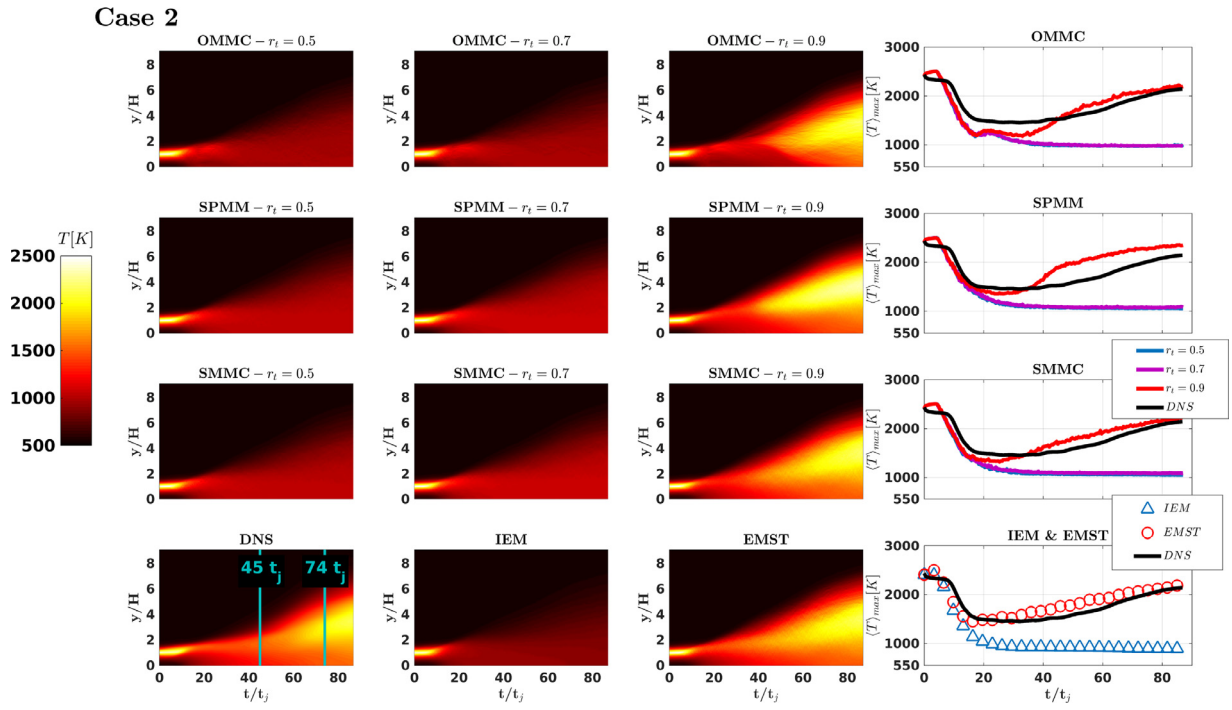

Fig. 6. Extinction and reignition events for Case 2. On the left is the contour coloured by mean temperature for the OMMC (first row), SPMM (second row) and SMMC (third row) model. On the right is the corresponding evolution of the maximum mean temperature in the domain. The results of the DNS, IEM and EMST model (last row) are also shown for reference.

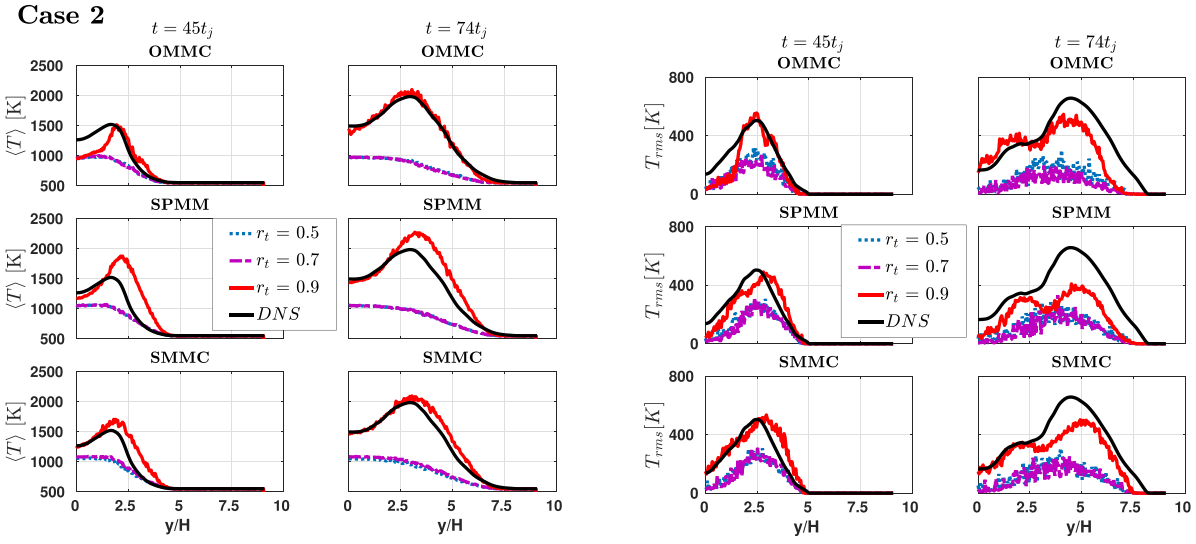

Fig. 7. Mean (left) and RMS (right) temperature comparison for the OMMC (first row), SPMM (second row) and SMMC (third row) model for Case 2 with $r_t = 0.5$, 0.7 and 0.9 at 45 and 74 characteristic jet times.

The profiles of $\langle T \rangle$ and T_{rms} at 45 and 74t_j for Case 2 are presented in Fig. 7. With $r_t = 0.9$, both SMMC and SPMM over-predict $\langle T \rangle$, while the SMMC exhibits a lower level of over-prediction compared to SPMM. The OMMC model with $r_t = 0.9$ yields near-perfect agreement with the DNS when the flame is fully reignited ($t = 74t_j$), but it under-predicts $\langle T \rangle$ near the jet core at $t = 45t_j$. For T_{rms}, all three MMC-like mixing models with $r_t = 0.5$ and 0.7 significantly under-predict T_{rms} since the flame is wrongly predicted to be fully extinguished. With $r_t = 0.9$, T_{rms} is reasonably well predicted at the beginning of the reignition event ($t = 45t_j$) while under-predicted at the jet edge when the flame is fully ignited ($t = 74t_j$).

For Case 3 with the highest extinction level, the DNS flame results show nearly global extinction. Only a weak reignition is observed at the end of simulation (around $t = 120t_j$). All three MMC-like mixing models fail to reproduce any sign of reignition with the selected r_t values. The reignition can not be reproduced with even higher localness, e.g., $r_t = 0.99$ (the results are not shown here). The IEM model predicts no reignition while the EMST model wrongly over-predicts the reignition and the flame to be in a fully-burning state. The over-prediction caused by the EMST model has been observed in [26] and attributed to the extreme localness resulting in a state where the notional particles are “stranded” in composition space.

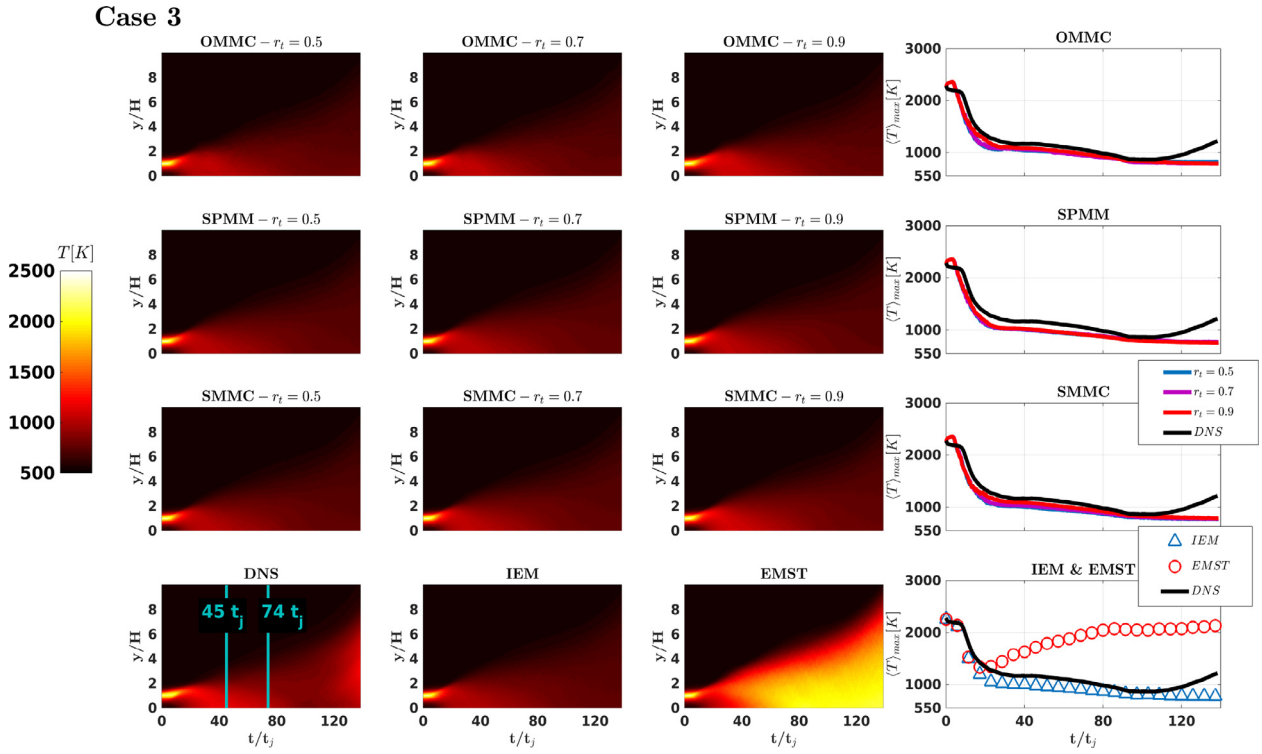

Fig. 8. Extinction and reignition events for Case 3. On the left is the contour coloured by mean temperature for the OMMC (first row), SPMM (second row) and SMMC (third row) model. On the right is the corresponding evolution of the maximum mean temperature in the domain. The results of the DNS, IEM and EMST model (last row) are also shown for reference.

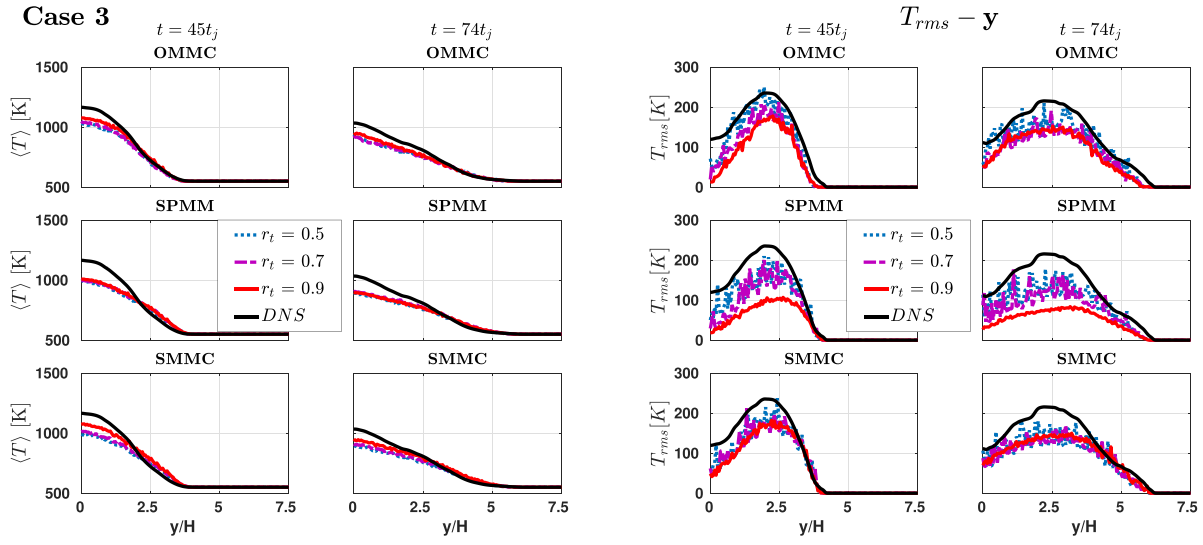

Fig. 9. Mean (left) and RMS (right) temperature comparison for the OMMC (first row), SPMM (second row) and SMMC (third row) model for Case 3 with $r_t = 0.5$, 0.7 and 0.9 at 45 and 74 characteristic jet times.

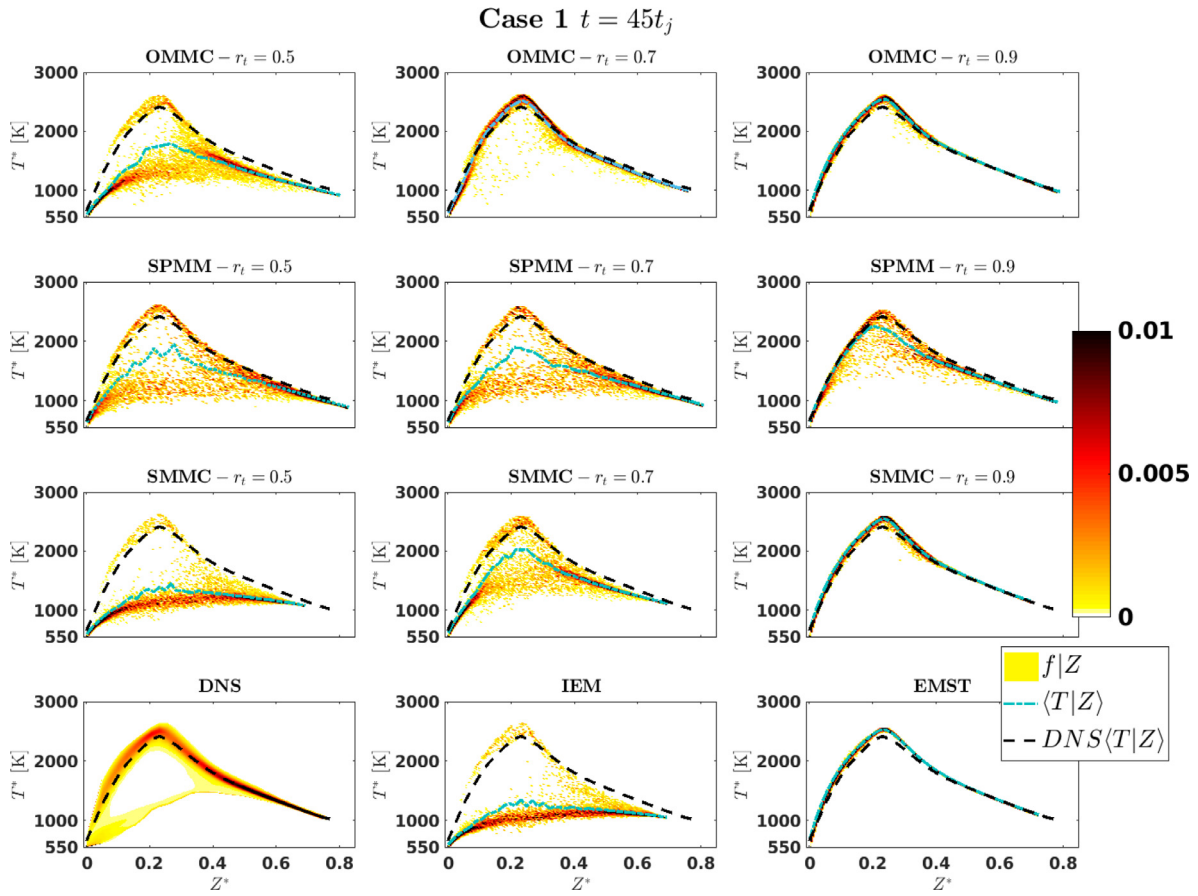

Fig. 10. Conditional probability density function of temperature on mixture fraction of OMMC (first row), SPMM (second row) and SMMC (third row) models for Case 1 at 45 characteristic jet times with $r_t = 0.5$, 0.7, 0.9, respectively. The results of DNS, IEM model and EMST model are also shown for reference.

According to Refs. [3,63], the weak reignition of the DNS in Case 3 is caused by a single, isolated reactive ignition kernel surviving the strained turbulent flow field. This suggests that the reignition may rely on the large-scale flow structure, which cannot be fully depicted by the current one-dimensional simulation. Another possible reason for no prediction of reignition by the MMC-like mixing models is that the prolonged delay between the extinction and reignition results in thorough mixing and thus a quasi-premixed reignition mode [3,63]. As the premixed flame imposes its own length and time scale, the single mixing time scale defined by mixture fraction may not be applicable to such phenomena. It may also be speculated that somewhat faster transport in physical space compared to the DNS (Fig. 2) might lead to lower gradients and hence lower mixture-fraction fluctuations, resulting in insufficient intermittency to represent both extinguished and burning states. However, Fig. 3 shows that some of the models predict the mixture-fraction variance quite well, yet still fail to predict the late-stage reignition, suggesting that some other explanation, such as those mentioned above, is the cause of the poor predictions in this extreme case.

For Case 3, T_{rms} is mainly contributed by turbulent mixing and its magnitude is much lower than that of Case 1 and 2, where chemical reaction is highly active. For the OMMC model, increasing r_t gradually dampens T_{rms} near jet core region ($y/H < 3.0$) at $45t_j$, and then the results show little dependence on r_t at $74t_j$. For the SPMM model, increasing r_t dampens T_{rms} at both $45t_j$ and $74t_j$. For the OMMC model, the prediction of T_{rms} shows little dependence on r_t. These trends of T_{rms} are qualitatively consistent with those of Z_{rms} as shown in Fig. 3. Such consistency can be attributed to the fact that the flame of Case 3 is near extinction and the reactive scalars (e.g., enthalpy) are similar to inert passive scalars (e.g., mixture fraction) in terms of mixing.

3.3. PDF and conditional fluctuations

Figures 10, 11 and 12 show scatter plots of temperature T^* versus mixture fraction Z^*. The particle data are coloured by the PDF of temperature conditioned on the mixture fraction $f|Z$. The conditional mean temperature, $\langle T|Z\rangle$, is also presented.

For Case 1, the DNS results exhibit a bimodal structure with distinct extinguished and burning branches. The bimodal structure is due to the fact that the ethylene flames have large effective Zel'dovich number (i.e., large activation energy) so that the extinguished and the burning states are clearly separated. The DNS $\langle T|Z\rangle$ profile suggests that the flame is almost fully ignited with a certain level of temperature variance around $\langle T|Z\rangle$, and with only a minority of particles dwelling on the extinguished branch. The MMC-like mixing models with a low level of localness ($r_t = 0.5$) correctly predict the two-branch flame structure, but the PDF particles are heavily weighted on the extinguished branch. As r_t increases ($r_t = 0.7$), the conditional mean temperature jumps from the extinguished branch to the burning branch, indicating an increasing level of ignition. With $r_t = 0.9$, which corresponds to a high level of localness, the MMC-like models adhere uniformly to the burning branch and the conditional mean temperature $\langle T|Z\rangle$ agrees well with the DNS result. For reference, the IEM model wrongly picks the extinguished branch, while the EMST model predicts the burning branch but with an extremely narrowed conditional PDF.

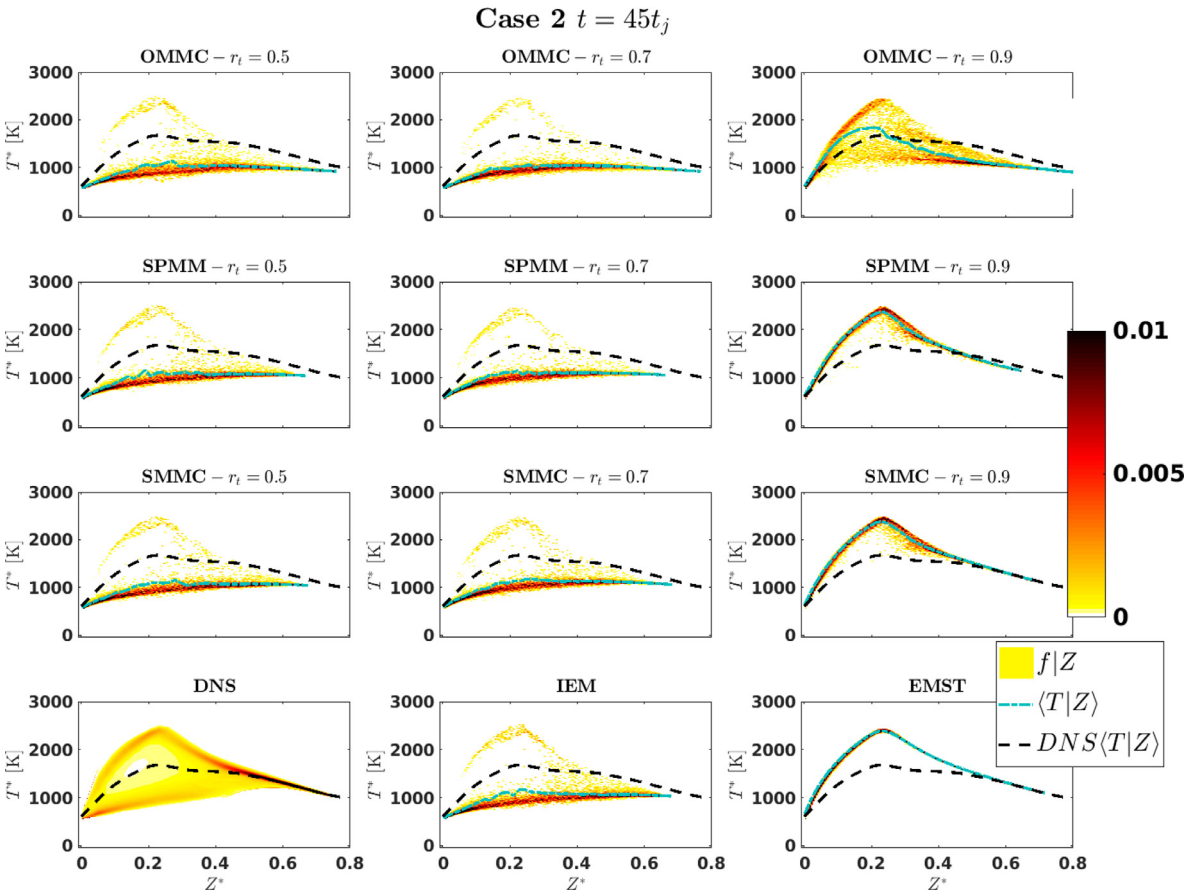

Fig. 11. Conditional probability density function of temperature on mixture fraction of OMMC (first row), SPMM (second row) and SMMC (third row) models for Case 2 at 45 characteristic jet times with $r_t = 0.5$, 0.7, 0.9, respectively. The results of DNS, IEM model and EMST model are also shown for reference.

For Case 2 with a decreased Damköhler number, the DNS results indicate a broad bimodal PDF. The DNS $\langle T|Z\rangle$ profile shows that the flame is neither fully ignited nor extinguished but characterised by an intermediate state. For all three MMC-like models, $r_t = 0.5$ and 0.7 predicts inadequate reignition. When $r_t = 0.9$, the SPMM and SMMC models over-predict the flame temperature to be on the fully burning branch. The result of the OMMC model with $r_t = 0.9$ resembles that of the DNS. For SPMM and SMMC, some intermediate values of r_t between 0.5 and 0.9 can reproduce the bimodal flame structure at $45t_j$, as will be shown later. Again, the IEM model predicts no reignition, similar to the MMC-like models with $r_t = 0.5$; the EMST model over-predicts the flame to be on the fully burning branch, similar to the MMC-like models with $r_t = 0.9$.

For Case 3, the DNS shows that the flame is almost globally extinguished. All three MMC-like models correctly predict the extinguished branch, and increasing r_t dampens the minor conditional fluctuation of temperature. The EMST model completely over-predicts the reignition and yields an over-narrowed PDF shape.

The width of the PDF as shown above can be quantified by the conditional RMS temperature profile, $\langle T_{rms}|Z\rangle$. Figure 13 shows the temporal evolution of $\langle T_{rms}|Z\rangle$, in mixture fraction space. Here the results of Case 2 are presented since it is characterised by a critical condition that the flame is at the edge of extinction. The evolution of the maximum value of $\langle T_{rms}|Z\rangle$ in the domain is also plotted in lateral view to characterise the level of conditional variance. The DNS shows that $\langle T_{rms}|Z\rangle$ is low in the laminar mixing stage, then rises due to the turbulent mixing, reaches the peak plateau when the flame starts to reignite, and finally decays as the burned mixture is homogenised to equilibrium state. The MMC-like models with $r_t = 0.5$ and 0.7 over-predict the peak of $\langle T_{rms}|Z\rangle$. The SMMC model with $r_t = 0.9$ under-predicts $\langle T_{rms}|Z\rangle$. The SPMM model with $r_t = 0.9$ yields a higher level of $\langle T_{rms}|Z\rangle$ but it over-predicts $\langle T|Z\rangle$. The OMMC model with $r_t = 0.9$ yields reasonably consistent result of $\langle T_{rms}|Z\rangle$ compared to the DNS.

Table 5
Suggested r_t values for Case 1 and 2.

	OMMC	SPMM	SMMC
Case 1 ($Da = 0.023$)	0.7	0.8	0.77
Case 2 ($Da = 0.017$)	0.8	0.89	0.86

The above results show that a high level of localness, e.g., $r_t = 0.9$, is needed to correctly predict the occurrence of extinction and reignition (e.g., $\langle T|Z\rangle$). However, $r_t = 0.9$ tends to over-dampen the conditional temperature fluctuations (e.g., $\langle T_{rms}|Z\rangle$) as shown by the SMMC and SPMM models. This motivates the improvement of the model performance by tuning r_t to achieve both correct $\langle T|Z\rangle$ and $\langle T_{rms}|Z\rangle$.

Here the value of r_t is tuned for the MMC models to further improve the prediction for $\langle T_{rms}|Z\rangle$. Figure 14 shows the results of $\langle T_{rms}|Z\rangle$ and $\langle T\rangle$ with the suggested r_t values listed in Table 5 for Case 1 and Case 2 (for Case 3 the occurrence of reignition is not correctly predicted and thus is not considered). These suggested r_t values are selected by trial-and-error to yield the closest resemblance (judged by eye) of $\langle T_{rms}|Z\rangle_{\max}$ to the DNS. It is seen that with the selected r_t values, all three MMC-like mixing models can yield reasonably correct flame structure. Meanwhile the occurrence of reignition events are correctly predicted. Of note is that as the extinction level increases (Damköhler number decreases), a higher

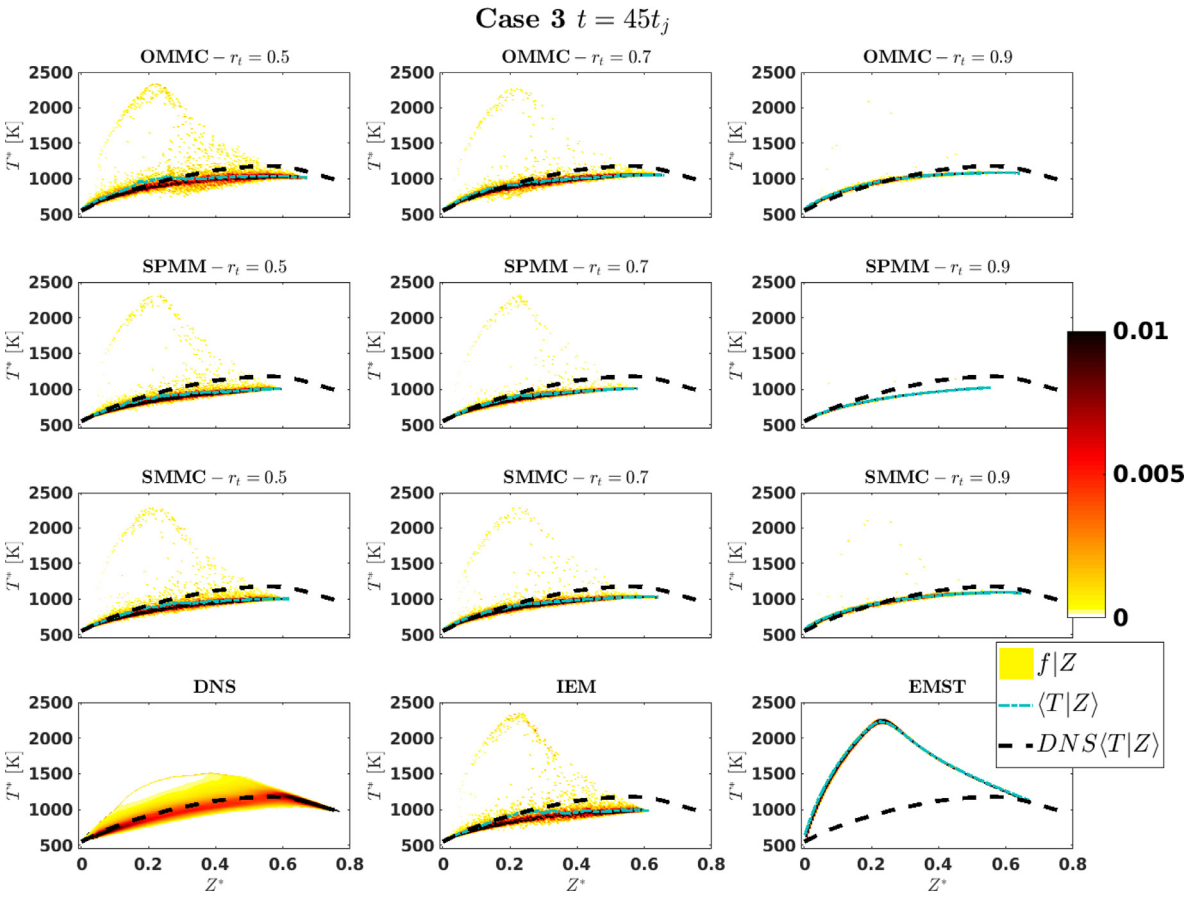

Fig. 12. Conditional probability density function of temperature on mixture fraction of OMMC (first row), SPMM (second row) and SMMC (third row) models for Case 3 at 45 characteristic jet times with $r_t = 0.5$, 0.7, 0.9, respectively. The results of DNS, IEM model and EMST model are also shown for reference.

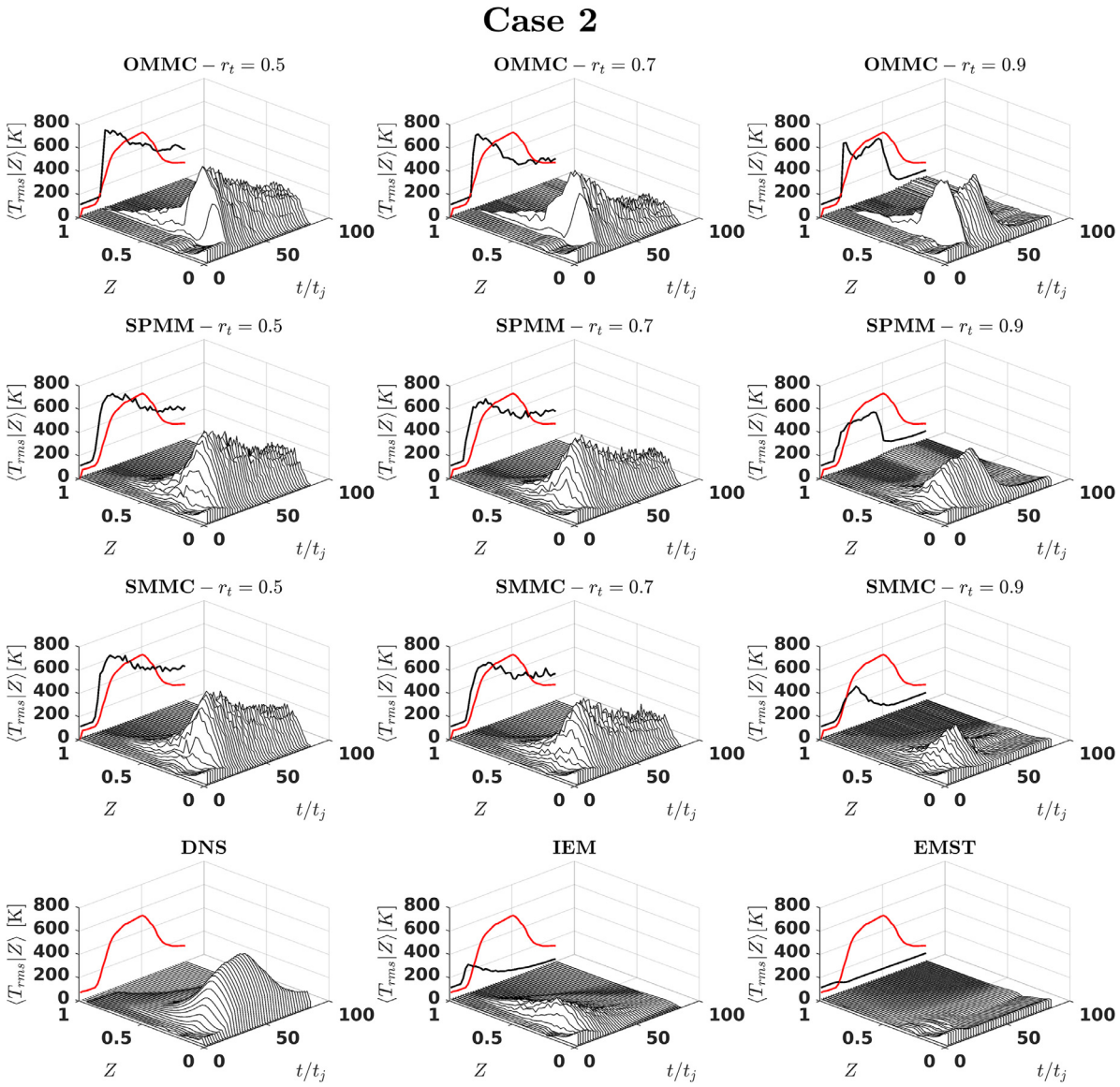

Fig. 13. Temporal evolution of conditional T_{rms} in mixture fraction space. The temporal evolution of the domain maximum $\langle T_{rms}|Z\rangle$ of the DNS is plotted (red line) in comparison to the result of each PDF mixing model (black line). (For interpretation of the references to colour in this figure legend, the reader is referred to the web version of this article.)

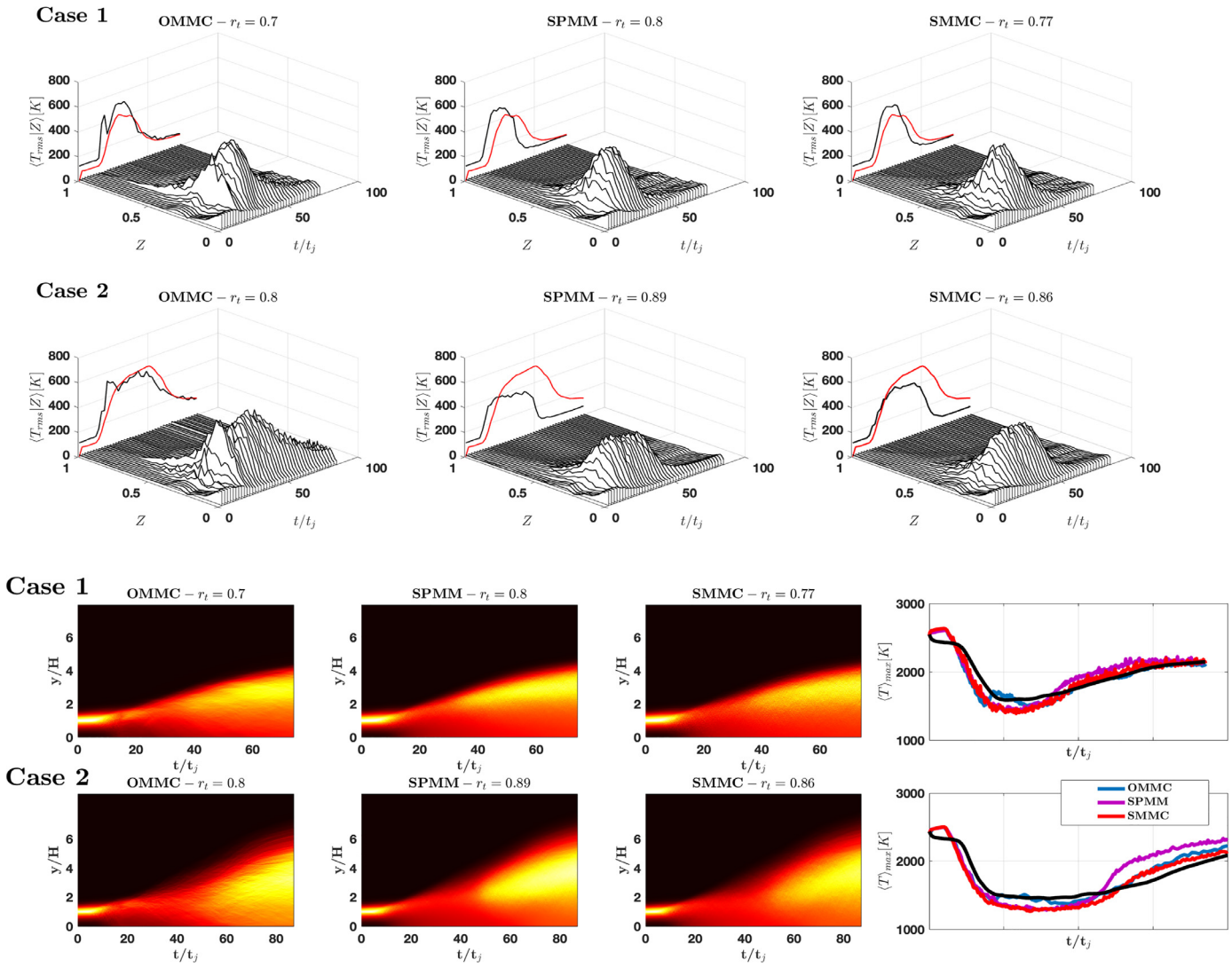

Fig. 14. Ignition behaviour of the three MMC-like mixing models with the suggested r_t values listed in Table 5. The upper figure set shows the evolution of $\langle T_{rms}|Z\rangle$. The temporal evolution of $\langle T_{rms}|Z\rangle_{\max}$ is plotted in red solid lines for DNS and TPDF, respectively, in the lateral plane. The lower figure set shows the contour of $\langle T\rangle$ and the evolution of $\langle T\rangle_{\max}$, to evidence the occurrence of reignition. For each figure set the results of Case 1 and 2 are plotted in the first and second row, respectively. (For interpretation of the references to colour in this figure legend, the reader is referred to the web version of this article.)

level of localness is needed by all three models to correctly predict both the occurrence of reignition and conditional flame structure. However, the values required are not the same between the models, despite all of them being determined in a consistent way.

4. Conclusions

The present work evaluated three MMC-like models for closing molecular mixing in the TPDF framework: OMMC, SPMM, and SMMC. The models were parameterised consistently in an idealised mean scalar gradient flow in order to achieve a specified scalar dissipation rate and to have explicit control over the models' localness, characterised by a target correlation coefficient between the MMC reference variable and mixture fraction.

The results of the models were compared to DNS of three turbulent nonpremixed ethylene flames featuring increasing levels of extinction and reignition. The mixing models were implemented in a RANS context, but with the turbulent flow field information, including the mean velocity, turbulent diffusion and mixing frequency directly extracted from the DNS, eliminating possible inaccuracies caused by the turbulence closure. Thus, the present results directly reveal the differences between the three MMC-like molecular mixing models and the effects of localness in the models.

For the prediction of flame extinction and reignition events, all three MMC-like mixing models show similar results that increasing localness yields prediction of stronger ignition. With a high level of localness ($r_t = 0.9$), all three MMC-like models agree well with the DNS flames on the overall progress of extinction and reignition.

When the conditional statistics are examined, it is found that the MMC-like mixing models can predict the bimodal PDF structure as exhibited by the DNS ethylene flames. When the level of localness ($r_t = 0.5$) is low, the predicted PDF particles are heavily weighted on the extinction branch, which is similar to the results with the IEM model. Increasing localness gradually makes PDF particles jump from the extinction branch to the fully burning branch, leading to a higher level of ignition. By choosing a suitable level of localness ($0.7 < r_t < 0.9$), the MMC-like models can correctly predict the overall ignition behaviour as well as the flame structure characterised by a broad bimodal PDF. When the localness continues to increase (e.g., $r_t = 0.9$ or higher), the MMC-like mixing models tend to overdamp the conditional fluctuations, similarly to the EMST model. A suggested r_t value for each test case and mixing

model is found to yield both correct reignition event and conditional flame structure. As the Damköhler number decreases from 0.023 to 0.017, the suggested r_t value increases from 0.7 to 0.8 for OMMC, 0.8 to 0.89 for SPMM and 0.77 to 0.86 for SMMC. This suggests that as the extinction level increases, a higher level of localness may be required to correctly predict both reignition event and conditional flame structure.

Overall the results demonstrate an advantage of the MMC-like mixing models over the conventional IEM and EMST model from the aspect of localness. The IEM model yields qualitatively correct predictions of the conditional fluctuation but fails to predict any sign of reignition. The EMST model can predict the overall ignition behaviour but significantly underestimates the conditional fluctuations. The MMC-like mixing models with high level of localness can achieve both correct ignition behaviour and correct level of conditional variances.

In terms of recommendations for model selection, the present results suggest that for the prediction of overall extinction and reignition behaviour, there is little to distinguish between the three MMC-like models, all of which can yield correct results with high level of localness with the suggested $r_t = 0.9$. When the flame structure, e.g., conditional variance statistics, is also of interest, r_t is suggested to be adjusted within the range of $0.7 < r_t < 0.9$ to yield a reasonable level of conditional variances. We found some evidence the optimal choice is flow-dependent, but further evidence will need to be accumulated to refine recommendations for parameter settings.

Notably, however, the OMMC and SMMC models both provide a better control of the scalar variance of mixture fraction and thus demonstrate better predictions than the current implementation of the SPMM model. For practical purposes, the implementation of the SMMC model is easier and more robust than the OMMC model, where numerical issues need to be taken care of to avoid the instabilities due to the correlation term for the modelling of particle velocity, and to deal with laminar cases. Considering the good prediction provided by SMMC, its simple and robust implementation, and its physically intuitive features, the SMMC model is recommended for modelling turbulent nonpremixed flames with significant extinction and reignition.

Future research could consider the following lines. First, if further evidence is accumulated that the mixing localness provided by MMC models needs to be flow dependent, it would be desirable that the model could adjust the relevant parameters, (e.g., r_t), by itself according to flow information, without user input. Since the reference variables are not physical variables, an entirely physics-based approach is not likely to be of much assistance in determining how to set r_t; instead, an experience-based approach is likely necessary. Second, the performance of SPMM model with regard to scalar variance control may be improved by adopting different canonical flow configurations to set its coefficients, or perhaps they could be set adaptively. Third, multiple reference variables, including progress variable and mixture fraction, may potentially be used to examine whether the reignition in Case 3 can be reproduced [64]. Fourth, the current assessment methodology could be extended to more complex flow configurations, e.g., 3D round jet flames, or flames including recirculation zones, where control of both conditional and unconditional variances may become more challenging. Finally, an equivalent effort should be directed towards the sparse MMC approaches in an LES context [42,65].

Novelty and significance statement

- The performance of three multiple mapping conditioning (MMC)-like mixing models is evaluated against DNS datasets featuring significant extinction and reignition.
- A unified approach is proposed to setting the parameters of the MMC-like mixing models. This approach allows specifiable dissipation rate and user-controllable localness.
- A hybrid evaluation strategy is adopted, with DNS datasets providing inputs such as turbulent diffusivity and mixing frequency, to eliminate possible sources of modelling error.
- The present work demonstrates an advantage of the MMC-like mixing models over the conventional IEM and EMST model with respect to controllable localness. Advantages and disadvantages of the different MMC-like formulations are discussed.

Declaration of Competing Interest

The authors declare that they have no known competing financial interests or personal relationships that could have appeared to influence the work reported in this paper.

CRediT authorship contribution statement

Zisen Li: Investigation, Validation, Writing – original draft. **Evatt R. Hawkes:** Conceptualization, Methodology, Supervision, Writing – review & editing. **Armin Wehrfritz:** Validation, Writing – review & editing. **Bruno Savard:** Writing – review & editing.

Acknowledgments

This work was supported by the Australian Research Council (ARC, DP180103923). Computational resources were provided by the Australian Government through the Pawsey Supercomputing Centre and the National Computational Infrastructure under the National Computational Merit Allocation Scheme, and by the University of New South Wales.

Supplementary material

Supplementary material associated with this article can be found, in the online version, at doi:10.1016/j.combustflame.2023.113039.

References

[1] E. Mastorakos, Ignition of turbulent non-premixed flames, Prog. Energy Combust. Sci. 35 (1) (2009) 57–97.
[2] E.R. Hawkes, R. Sankaran, J.H. Chen, A study of extinction and reignition dynamics in syngas jet flames using terascale direct numerical simulations: sensitivity to the choice of reacting scalar, Proc. Aust. Combust. Symp. (1) (2007) 46–49.
[3] D.O. Lignell, J.H. Chen, H.A. Schmutz, et al., Effects of Damköhler number on flame extinction and reignition in turbulent non-premixed flames using DNS, Combust. Flame 158 (5) (2011) 949–963, doi:10.1016/j.combustflame.2010.10.027.
[4] Y. Yang, H. Wang, S.B. Pope, J.H. Chen, Large-eddy simulation/probability density function modeling of a non-premixed CO/H_2 temporally evolving jet flame, Proc. Combust. Inst. 34 (1) (2013) 1241–1249.
[5] S.B. Pope, PDF methods for turbulent reactive flows, Prog. Energy Combust. Sci. 11 (2) (1985) 119–192, doi:10.1016/0360-1285(85)90002-4.
[6] S.B. Pope, Simple models of turbulent flows, Phys. Fluids 23 (1) (2011) 011301, doi:10.1063/1.3531744.
[7] D.C. Haworth, Progress in probability density function methods for turbulent reacting flows, Prog. Energy Combust. Sci. 36 (2) (2010) 168–259, doi:10.1016/j.pecs.2009.09.003.
[8] S.B. Pope, A model for turbulent mixing based on shadow-position conditioning, Phys. Fluids 25 (11) (2013) 110803, doi:10.1063/1.4818981.
[9] Y. Pei, E.R. Hawkes, M. Bolla, S. Kook, G.M. Goldin, Y. Yang, S.B. Pope, S. Som, Modelling *n*-dodecane spray and combustion with the transported probability density function method, Combust. Flame 168 (2016) 420–435.
[10] C. Straub, S. De, A. Kronenburg, K. Vogiatzaki, The effect of timescale variation in multiple mapping conditioning mixing of PDF calculations for Sandia Flame series D–F, Combust. Theory Model. 20 (5) (2016) 894–912, doi:10.1080/13647830.2016.1191677.
[11] C. Straub, A. Kronenburg, O.T. Stein, R.S. Barlow, D. Geyer, Modeling stratified flames with and without shear using multiple mapping conditioning, Proc. Combust. Inst. 37 (2) (2019) 2317–2324.

[12] S. Vo, A. Kronenburg, O.T. Stein, M.J. Cleary, et al., Multiple mapping conditioning for silica nanoparticle nucleation in turbulent flows, Proc. Combust. Inst. 36 (1) (2017) 1089–1097, doi:10.1016/j.proci.2016.08.088.

[13] Y. Shoraka, S. Galindo-Lopez, M.J. Cleary, A.R. Masri, F. Salehi, A.Y. Klimenko, Modelling of a turbulent premixed flame series using a new MMC-LES model with a shadow position reference variable, Proc. Combust. Inst. 38 (2021) 3057–3065.

[14] S. Vo, O.T. Stein, A. Kronenburg, M.J. Cleary, et al., Assessment of mixing time scales for a sparse particle method, Combust. Flame 179 (2017) 280–299, doi:10.1016/j.combustflame.2017.02.017.

[15] Z. Huang, M.J. Cleary, Z. Ren, H. Zhang, et al., Large eddy simulation of a supersonic lifted hydrogen flame with sparse-Lagrangian multiple mapping conditioning approach, Combust. Flame 238 (2022) 111756.

[16] J. Villermaux, J. C. Devillon, in: Proc. 2nd Int. Symp. on Chem. reaction Eng. (1) (1972) 1–13. 10.1016/j.proci.2012.09.009.

[17] T.S. Lundgren, Model equation for nonhomogeneous turbulence, Phys. Fluids 12 (3) (1969) 485–497, doi:10.1063/1.1692511.

[18] J. Janicka, W. Kolbe, W. Kollmann, Closure of the transport equation for the probability density function of turbulent scalar fields, J. Non-Equilib. Thermodyn. 4 (1) (2009) 47–66, doi:10.1515/jnet.1979.4.1.47.

[19] S. Subramaniam, S.B. Pope, A mixing model for turbulent reactive flows based on Euclidean minimum spanning trees, Combust. Flame 115 (4) (1998) 487–514, doi:10.1016/S0010-2180(98)00023-6.

[20] A.Y. Klimenko, S.B. Pope, The modeling of turbulent reactive flows based on multiple mapping conditioning, Phys. Fluids 15 (7) (2003) 1907–1925, doi:10.1063/1.1575754.

[21] S. Subramaniam, S.B. Pope, Comparison of mixing model performance for nonpremixed turbulent reactive flow, Combust. Flame 117 (4) (1999) 732–754, doi:10.1016/S0010-2180(98)00135-7.

[22] R. McDermott, S.B. Pope, A particle formulation for treating differential diffusion in filtered density function methods, J. Comput. Phys. 226 (1) (2007) 947–993, doi:10.1016/j.jcp.2007.05.006.

[23] A.Y. Klimenko, S.B. Pope, Propagation speed of combustion and invasion waves in stochastic simulations with competitive mixing, Combust. Theory Model. 16 (4) (2012) 679–714.

[24] A.T. Norris, S.B. Pope, Turbulent mixing model based on ordered pairing, Combust. Flame 83 (1) (1991) 27–42, doi:10.1016/0010-2180(91)90201-L.

[25] B. Merci, D. Roekaerts, B. Naud, Study of the performance of three micromixing models in transported scalar PDF simulations of a piloted jet diffusion flame (æ delft flame IIIg), Combust. Flame 144 (3) (2006) 476–493.

[26] A. Krisman, J.C.K. Tang, E.R. Hawkes, D.O. Lignell, J.H. Chen, A DNS evaluation of mixing models for transported PDF modelling of turbulent nonpremixed flames, Combust. Flame 161 (8) (2014) 2085–2106, doi:10.1016/j.combustflame.2014.01.009.

[27] M.J. Cleary, A. Kronenburg, Hybrid multiple mapping conditioning on passive and reactive scalars, Combust. Flame 151 (4) (2007) 623–638, doi:10.1016/j.combustflame.2007.07.008.

[28] K. Vogiatzaki, A. Kronenburg, S. Navarro-Martinez, W.P. Jones, Stochastic multiple mapping conditioning for a piloted, turbulent jet diffusion flame, Proc. Combust. Inst. 33 (1) (2011) 1523–1531.

[29] A. Kronenburg, M.J. Cleary, Multiple mapping conditioning for flames with partial premixing, Combust. Flame 155 (1) (2008) 215–231, doi:10.1016/j.combustflame.2008.03.012.

[30] B. Sundaram, A.Y. Klimenko, M.J. Cleary, U. Maas, et al., Prediction of NOx in premixed high-pressure lean methane flames with a MMC-partially stirred reactor, Proc. Combust. Inst. 35 (2) (2015) 1517–1525, doi:10.1016/j.proci.2014.07.069.

[31] C. Straub, A. Kronenburg, O.T. Stein, G. Kuenne, J. Janicka, R.S. Barlow, D. Geyer, et al., Multiple mapping conditioning coupled with an artificially thickened flame model for turbulent premixed combustion, Combust. Flame 196 (2018) 325–336, doi:10.1016/j.combustflame.2018.05.021.

[32] A.P. Wandel, A.Y. Klimenko, Testing multiple mapping conditioning mixing for Monte Carlo probability density function simulations, Phys. Fluids 17 (12) (2005) 128105, doi:10.1063/1.2147609.

[33] A.P. Wandel, Conditional dissipation of scalars in homogeneous turbulence: closure for MMC modelling, Combust. Theory Model. 17 (4) (2013) 707–748.

[34] K. Vogiatzaki, S. Navarro-Martinez, S. De, A. Kronenburg, et al., Mixing modelling framework based on multiple mapping conditioning for the prediction of turbulent flame extinction, Flow Turbul. Combust. 95 (2015) 501–517.

[35] S.K. Ghai, S. De, A. Kronenburg, Numerical simulations of turbulent lifted jet diffusion flames in a vitiated coflow using the stochastic multiple mapping conditioning approach, Proc. Combust. Inst. 37 (2019) 2199–2206.

[36] Z. Huo, F. Salehi, S. Galindo-Lopez, M.J. Cleary, A.R. Masri, et al., Sparse MMC-LES of a Sydney swirl flame 37 (2) (2019) 2191–2198, doi:10.1016/j.proci.2018.06.193.

[37] B. Sundaram, A.Y. Klimenko, A PDF approach to thin premixed flamelets using multiple mapping conditioning, Proc. Combust. Inst. 36 (2) (2017) 1937–1945, doi:10.1016/j.proci.2016.07.116.

[38] S.K. Ghai, S. De, Numerical modeling of turbulent premixed combustion using RANS based stochastic multiple mapping conditioning approach, Proc. Combust. Inst. 37 (2019) 2519–2526.

[39] S. Galindo, F. Salehi, M.J. Cleary, A.R. Masri, et al., MMC-LES simulations of turbulent piloted flames with varying levels of inlet inhomogeneity, Proc. Combust. Inst. 36 (2) (2017) 1759–1766, doi:10.1016/j.proci.2016.07.055.

[40] A. Varna, M.J. Cleary, E.R. Hawkes, et al., A multiple mapping conditioning mixing model with a mixture-fraction like reference variable. Part 1: model derivation and ideal flow test cases, Combust. Flame 181 (2017) 342–353, doi:10.1016/j.combustflame.2017.03.016.

[41] A. Varna, M.J. Cleary, E.R. Hawkes, et al., A multiple mapping conditioning mixing model with a mixture-fraction like reference variable. Part 2: RANS implementation and validation against a turbulent jet flame, Combust. Flame 181 (2017) 354–364, doi:10.1016/j.combustflame.2017.03.017.

[42] M.J. Cleary, A.Y. Klimenko, J. Janicka, M. Pfitzner, et al., A sparse-Lagrangian multiple mapping conditioning model for turbulent diffusion flames, Proc. Combust. Inst. 32 (1) (2009) 1499–1507, doi:10.1016/j.proci.2008.07.015.

[43] A.P. Wandel, R.P. Lindstedt, Hybrid binomial Langevin-multiple mapping conditioning modeling of a reacting mixing layer, Phys. Fluids 21 (1) (2009) 015103, doi:10.1063/1.3041716.

[44] A.P. Wandel, R.P. Lindstedt, A mixture-fraction-based hybrid binomial Langevin-multiple mapping conditioning model, Proc. Combust. Inst. 37 (2018) 2151–2158, doi:10.1016/j.proci.2018.06.122.

[45] X.Y. Zhao, A. Bhagatwala, J.H. Chen, D.C. Haworth, S.B. Pope, et al., An a priori DNS study of the shadow-position mixing model, Combust. Flame 165 (2016) 223–245, doi:10.1016/j.combustflame.2015.12.009.

[46] J.C.K. Tang, A. Kong, E.R. Hawkes, S.B. Pope, J.H. Chen, Evaluating the shadow position mixing model for transported PDF modeling of non-premixed flames, Australasian Fluid Mechanics Conference (2017).

[47] A. Varna, A. Wehrfritz, R.H. Evatt, J.C. Matthew, T. Lucchini, G. D'Errico, S. Kook, N.C. Qing, et al., Application of a multiple mapping conditioning mixing model to ECN Spray A, Proc. Combust. Inst. 37 (3) (2019) 3263–3270, doi:10.1016/j.proci.2018.06.007.

[48] C.K.T. Joshua, H. Wang, M. Bolla, A. Wehrfritz, R.H. Evatt, A DNS evaluation of mixing and evaporation models for TPDF modelling of nonpremixed spray flames, Proc. Combust. Inst. 37 (2018) 3363–3372.

[49] S. Galindo-Lopez, F. Salehi, M.J. Cleary, A.R. Masri, G. Neuber, O.T. Stein, A. Kronenburg, A. Varna, E.R. Hawkes, B. Sundaram, A.Y. Klimenko, Y. Ge, A stochastic multiple mapping conditioning computational model in OpenFOAM for turbulent combustion, Comput. Fluids 172 (2018) 410–425.

[50] P. Simatos, L. Tian, R.P. Lindstedt, The impact of molecular diffusion on auto-ignition in a turbulent flow, Combust. Flame 239 (2022) 111665.

[51] R. Cabra, J.-Y. Chen, R.W. Dibble, A.N. Karpetis, R.S. Barlow, Lifted methane–air jet flames in a vitiated coflow, Combust. Flame 143 (4) (2005) 491–506.

[52] M. Kuron, E.R. Hawkes, Z. Ren, J.C.K. Tang, H. Zhou, J.H. Chen, T. Lu, et al., Performance of transported PDF mixing models in a turbulent premixed flame, Proc. Combust. Inst. 36 (2) (2017) 1987–1995.

[53] M. Kuron, Z. Ren, E.R. Hawkes, H. Zhou, H. Kolla, J.H. Chen, T. Lu, A mixing timescale model for TPDF simulations of turbulent premixed flames, Combust. Flame 177 (2017) 171–183, doi:10.1016/j.combustflame.2016.12.011.

[54] Z. Ren, S. Subramaniam, S. Pope, Implementation of the EMST mixing model(http://tcg.mae.cornell.edu/emst) (2002).

[55] W.P. Jones, B.E. Launder, The prediction of laminarization with a two-equation model of turbulence, Int. J. Heat Mass Transf. 15 (2) (1972) 301–314, doi:10.1016/0017-9310(72)90076-2.

[56] S.B. Pope, Turbulent flows, Cambridge University Press, New York, U.S., 2000.

[57] P. Sagaut, Large eddy simulation for incompressible flows, Springer Verlag Press, Berlin, Germany, 2006.

[58] R.R. Cao, H. Wang, S.B. Pope, The effect of mixing models in PDF calculations of piloted jet flames, Proc. Combust. Inst. 31 (1) (2007) 1543–1550, doi:10.1016/j.proci.2006.08.052.

[59] S. Corrsin, The decay of isotropic temperature fluctuations in an isotropic turbulence, Aeronaut. J. 18 (6) (1951) 417–423, doi:10.2514/8.1982.

[60] Documents of cubic smoothing spline algorithm(https://www.mathworks.com/help/curvefit/csaps.html)(Accessed 2023).

[61] C. de Boor, A practical guide to splines, Springer-Verlag, New York, 1980.

[62] S. Viswanathan, H. Wang, S.B. Pope, et al., Numerical implementation of mixing and molecular transport in LES/PDF studies of turbulent reacting flows, J. Comput. Phys. 230 (17) (2011) 6916–6957, doi:10.1016/j.jcp.2011.05.020.

[63] D.O. Lignell, D.S. Rappleye, One-dimensional-turbulence simulation of flame extinction and reignition in planar ethylene jet flames, Combust. Flame 159 (9) (2012) 2930–2943, doi:10.1016/j.combustflame.2012.03.018.

[64] C. Yu, P. Breda, M. Pfitzner, U. Maas, The hierarchy of low-dimensional manifolds in the context of multiple mapping conditioning mixing model, Proc. Combust. Inst. 39 (2022) 2299–2309.

[65] M.J. Cleary, A.Y. Klimenko, A generalised multiple mapping conditioning approach for turbulent combustion, Flow Turbul. Combust. 82 (4) (2009) 477–491.